NBSIR 84-3012

Second Interim Progress Report: MATERIALS SELECTION CRITERIA FOR CRACK ARRESTER STRAKES IN NAVAL VESSELS

National Bureau of Standards
U.S. Department of Commerce
Boulder, CO 80303

October 1984

NBSIR 84-3012

Second Interim Progress Report: MATERIALS SELECTION CRITERIA FOR CRACK ARRESTER STRAKES IN NAVAL VESSELS

R.B. King
T. Teramoto
D.T. Read

Fracture and Deformation Division
Center for Materials Science
National Bureau of Standards
U.S. Department of Commerce
Boulder, CO 80303

October 1984

Sponsored by:
Naval Sea Systems Command (SEA05R25)

Directed by:
David Taylor Naval Ship R&D Center

U.S. DEPARTMENT OF COMMERCE, Malcolm Baldrige, Secretary

NATIONAL BUREAU OF STANDARDS, Ernest Ambler, Director

Materials Selection Criteria for Crack Arrester Strakes in Naval Vessels: Second Interim Progress Report

R. B. King, T. Teramoto, and D. T. Read

Fracture and Deformation Division
National Bureau of Standards
Boulder, Colorado 80303

The phenomenon of crack arrest, in which a crack propagates through a brittle material, encounters a high toughness material, and stops has been studied. This phenomenon is of practical importance in understanding crack arrest in ship structures. Laboratory experiments have been conducted under conditions intended to simulate those in a structural situation.

These experiments were designed to include two key features of ship structural behavior: 1) Crack arrest occurs specifically because a step in toughness is encountered; 2) the load on the specimen, simulating dead load in the structure, is transferred to the uncracked ligament after arrest, thus introducing the possibility of reinitiation. A spring-loaded double-cantilever-beam (DCB) specimen has been used in these experiments. An electron-beam weld is made along the crack propagation line, producing a brittle crack propagation path with a step in toughness at its end.

The dynamic run-arrest portion of these experiments has been modeled using a modification of Kanninen's DCB model that includes the effect of the loading spring, and using a finite element model. The elastic-plastic reloading portion has been modeled quasistatically using J integral and tearing instability theory. In addition, a simplified dynamic viscoelastic-plastic model has been developed to analyze the reloading portion of the experiments.

Results of this program are intended to indicate quantitatively whether a candidate arrester material will arrest a crack at service temperatures and subsequently prevent reinitiation.

Key words: crack arrest; crack propagation; dynamic fracture; dynamic toughness; elastic-plastic fracture; toughness

INTRODUCTION

This report describes progress on the research program "Materials Selection Criteria for Crack Arrester Strakes in Naval Vessels." This is the second interim progress report covering this program. In the first report, results of an extensive literature survey on research relevant to this program were presented, and research plans were described [1]. In the period described by the present report, progress has been made in several areas: 1) A specimen design has been developed that permits laboratory simulation of the key features of crack propagation and arrest in ships. 2) Analytical models sufficient to characterize the specimen have been developed. 3) Extensive experimental results have been obtained using EH36 steel and HY80 steel. In this report, crack propagation and arrest, as are likely to occur in ships, are described; the specimen design and analytical models are discussed; and the procedures and experimental results are presented.

In a worst case fracture event in a ship, the crack may propagate long distances before encountering an arrester. Dynamic effects become important in such a "long crack jump" event [2]. A large percentage of the service stress driving the crack in the ship is likely to result from dead loading, and thus from a quasistatic analysis it would be expected that the crack would be propagating under severely growing stress intensity conditions. However, inertia effects tend to offset the expected growth of stress intensity, because of large and rapid compliance increases resulting from crack propagation. These compliance changes necessitate significant structural motion to maintain load; this motion cannot occur instantaneously. Nevertheless, crack arrest does not occur because of decaying stress intensity in the actual ship; instead it occurs specifically because a step increase in material toughness is encountered at the arrester interface.

After arrest, the uncracked ligament is reloaded to a higher stress than before cracking. The possibility exists of overloading the ligament because of the large area loss caused by a long crack jump. This was alluded to in [2], where it was pointed out that "another concern is the possibility that the arrester, after temporarily stopping a crack, will fail in gross yielding as the loads on the ship hull are redistributed." In addition to gross yielding, however, there is the possibility that the crack, which after load redistribution is likely to be surrounded by a large plastic strain field, will reinitiate and propagate through the arrester in ductile tearing.

Successful performance in the arrester application consists of two steps: 1) The crack propagation through the hull steel will be largely in the cleavage mode, with some accompanying ductile ligaments [3, 4] and shear lips [5]. In order to cause arrest, the arrester steel must be sufficiently tough and have a low enough ductile to brittle transition temperature to force a fracture mode change from cleavage to tearing. 2) The arrester must be able to resist failure by reinitiation in tearing. This necessitates a high tearing modulus, to prevent unstable tearing and to provide high resistance to stable tearing, so tearing cannot propagate through the finite-width arrester strake.

The experiments described in this paper were designed to incorporate the features described above of crack propagation and arrest in ships. Before describing the experiments, a review is made of relevant theory on dynamic crack propagation, and previous experimental work on crack arrest at a high toughness interface is described.

THEORETICAL BACKGROUND

A literature review of research relevant to the current program was described in [1], where an extensive review of the theory of dynamic crack

arrest was presented. Key results from the theory are summarized here for completeness. In crack propagation and arrest in both ships and in the experiments described in this paper, the crack propagates through a brittle material and then encounters a higher toughness material, whereupon arrest may occur. The extent of the plastic deformation accompanying propagation through the brittle material is considered to be sufficiently small to permit the use of dynamic linear-elastic fracture mechanics (LEFM). More widespread plasticity may occur after the crack has encountered the ductile material, however, so that the final stage of the run-arrest event requires description by elastic-plastic fracture mechanics (EPFM).

Dynamic LEFM theory is based on a generalization of the Griffifth-Irwin-Orowan fracture criterion [2]. The condition for crack propagation is

$$G \geq R \tag{1}$$

where

$$G = - 1/B \, (-dW/da + dU/da + dT/da) \; ; \tag{2}$$

G is the dynamic energy-release rate, a is the instantaneous crack length, B is the thickness at the crack tip, and W, U, and T represent the work done by the applied loads, the specimen's stored strain energy and the total kinetic energy, respectively. The dynamic toughness of the material is characterized by the parameter R. To account for possible strain-rate effects in the high strain-gradient region near the crack tip [5], R is taken to be a function of the crack speed. A near-tip evaluation of G establishes the relation between G and the dynamic stress-intensity factor, K [6]:

$$G = [(1-\nu^2)/E]A(\dot{a}) \, K^2 \tag{3}$$

where $A(\dot{a})$ is a geometry-independent function of crack speed $\dot{a}$, ν is Poisson's ratio, E is Young's modulus, and K, the stress intensity factor, is the coefficient of the singular term of an expansion of the mode I elastic stress field in the near-tip region of the moving crack. Making use of eq (3),the crack propagation criterion eq (1) may be replaced by the equivalent condition

$$K \geq K_D(\dot{a}) \tag{4}$$

A schematic plot of K_D, the dynamic material fracture resistance, as a function of $\dot{a}$ is shown in figure 1. Except at very high crack speeds, the value of K_D is less than the static initiation toughness, K_c, so that less driving force is required to maintain continued crack propagation than to initiate crack extension.

From a dynamic solution for propagation of a semi-infinite crack in an infinite body, Freund [6] has shown that the value of the stress intensity factor after arrest is equal to the statically computed value for the same body. This result will also be true for finite bodies if the duration of the run-arrest event is short enough that wave reflection from the boundaries does not have time to occur. This explains the experimental results of Kihara et al [7], who found that a static computation of K was sufficient to predict the results of a crack arrest test as long as the crack propagation length was short. For longer crack jumps, however, serious discrepancy arose between the static calculation and experimental results. This phenomenon was studied in detail by Kanazawa et al [8], who in successive experiments systematically varied the distance from the crack plane to the specimen boundaries where significant wave interaction was occurring. Crack propagation lengths in a

ship may be long, and structural details are present from which wave reflections are likely to occur. Specimens intended to simulate crack propagation in ships should therefore be designed so that significant wave interaction with the boundaries of the specimen does occur during testing.

The value of K as a function of time during a test can be calculated from a dynamic LEFM analysis of the specimen. From this and the crack growth history a(t), the resistance K_D can be inferred, if it is assumed that the equality in eq (4) holds.

If, when the propagating crack encounters the tough material of the arrester, significant plastic deformation occurs during the arrest process, then dynamic LEFM may be invalidated. This portion of the run-arrest event may therefore require EPFM analysis. This is a difficult problem because dynamic elastic-plastic analysis is significantly more complicated than elastic analysis. In addition, it has not been established which driving force parameter is most suitable for characterizing crack propagation under elastic-plastic conditions. Several candidate parameters, such as the J integral, Crack Opening Displacement (COD), and Crack Opening Angle (COA), may be generalizable to the dynamic crack propagation case, but this has not yet been proven. At present, it appears most likely that a near-tip deformation parameter such as COD or COA will be suitable for the dynamic running crack case [9].

The difficulty of EPFM analysis is alleviated somewhat for the application in the current program, because the experimental results in this paper appear to justify a simplified theoretical approach: The initial run-arrest event occurs at a high speed but is accompanied by relatively little plastic deformation; thus it can be characterized by LEFM. After arrest,the plastic deformation is extensive but occurs relatively slowly, and

thus from quasistatic reasoning, parameters like the J integral and tearing modulus are appropriate to characterize the reinitiation portion of these tests. Because, as will be demonstrated under Experimental Results, a relatively large amount of stable tearing (40 to 50 mm) typically occurs in the reinitation phase of these tests, the rigorous validity of J and T as characterizing parameters is in question [10]. Nevertheless, these parameters provide at least a good qualitative basis for assesssing the driving-force conditions in these tests in the reinitiation phase.

SPECIMEN AND APPARATUS DESIGN

Before designing a specimen configuration, a literature review was performed of experimental work relevant to crack arrest by high toughness arresters in ship structures. Results of this literature survey are presented in [1] and are summarized here for completeness. Most of the recent work directed towards studying crack arrest at a high toughness interface under conditions similar to those in ships has been conducted in Japan [7,8,11,12]. Large duplex specimens, typically of the "double-tension" type (fig. 2) have been employed. Crack propagation is initiated in a brittle starter section. This section is welded to the arrester material under study. The main tensile load applied in these tests simulates service stresses in a structure. Load drop during the run-arrest event in these tests has been found experimentally to be minimal [12] and arrest does occur under rising stress intensity conditions. However, significant load drop will occur after arrest because the large testing machines used are effectively under fixed-grip conditions. Thus, dynamic load redistribution to the uncracked ligament is not present in these tests. Another drawback to the use of large duplex specimens of the type described is that it is difficult to channel crack propagation. Turning and branching often occur in the starter section resulting in arrest which is not caused by the arrester material [11].

The specimen design used in the tests described in this paper was intended to eliminate some of the drawbacks cited for the large-scale duplex specimens. A spring-loaded double-cantilever beam (DCB) configuration was chosen (fig. 3). The DCB configuration is desirable because high crack propagation lengths can be achieved under relatively low loads. However, this specimen undergoes large compliance changes during crack propagation, thus the spring in the load train is necessary to prevent severe load drop. The loading spring was constructed using Belleville disk washers. It has a stiffness of 2.04 kN/mm per washer (the number of washers used varied between 8 and 16) and a load capacity of 410 kN.

To prevent the problem of turning or branching in the starter section a duplex configuration was not used. Instead, the specimens were machined entirely of ductile material. A brittle crack propagation path was provided by placing an electron-beam weld along the crack line. This relatively brittle weld tends to channel the crack propagation along a straight line, and a step in toughness is present at the end of the weld.

A key feature of the double-tension specimen was provided in this specimen by machining a pocket into which a hydraulic jack is placed. The jack loading is very stiff, effectively fixed grip. It decays very rapidly as crack propagation occurs and has essentially vanished by the time the crack has propagated to the end of the weld. Desired conditions at arrest can thus be provided by adjusting the main load applied through the loading spring, while initiation conditions are independently controlled by adjusting the jack load.

The following instrumentation was used on the specimen: load was monitored using the testing machine's load cell output, after amplification by a signal conditioner. Crack position as a function of time was detected using resistive trip-wire gages. In the first two tests reported here, these gages

were made using conductive paint lines. In subsequent tests commercial crack detector gages were used. The latter approach was more satisfactory. Typical locations of the trip-wire gages are shown in figure 4. To study the evolution of the plastic deformation in the ligament as a function of time, strain gages were also placed at selected locations in this region (fig. 4). Since the uncracked ligament is loaded primarily in bending, a Green and Hundy [13] type slip-band pattern was expected. This was confirmed using a quasi-static finite element model of the specimen. The strain gages were intended to be placed in the path of the slip band development.

Transient data from all instruments were collected using several digital oscilloscopes. Digitizing rates ranged from 10 microseconds per point for the slowest signals studied to 0.5 microseconds per point for the fastest. Triggering was achieved using a trip-wire gage located approximately 10mm from the crack tip. Prior to initiation, temperatures in the specimen were monitored using two thermocouples, one placed in the vicinity of the starter notch tip in the electron beam weld and the other near the end of the weld in the base metal.

The experiments on EH36 were used for test method development. Three different specimen configurations were used in the tests on EH36. The specimen dimensions are shown in figure 5. Several considerations affected specimen dimensions. The loading spring used was capable of applying 410,000 N. The beam arm heights were chosen so that they would not yield under this load during crack propagation. This was intended to reduce the possibility of crack turning. The length of the specimen was determined by choosing a desired crack jump length, estimating the starter notch length needed to reach the initiation toughness value, and sizing the uncracked ligament width. In the first two tests, this width was chosen so that the load at at net section

yield would be equal to the applied load at arrest computed quasistatically. In all subsequent tests the ligament widths was chosen so that the net section yield load was significantly less than the applied load at arrest computed quasistatically. As discussed in the section on analysis, the value of the J integral in the specimen after arrest was computed statically and the ligament width was chosen such that significant ductile tearing would occur after arrest.

In estimating the applied load at arrest, unloading of the load spring was accounted for quasistatically by calculating the compliance change in the specimen between the initial and final crack lengths. The quasistatic calculation predicted load drops of 5-10% in the geometries tested. Based on the considerations described, the tapered design of specimen 1 resulted in smaller specimen dimensions for a given crack jump length. It was later decided that this advantage was outweighed by the additional analytical complexity caused by the nonprismatic beam arms. Two different rectangular specimen sizes were tested in the EH36 series to achieve different crack jump lengths. Because the results of the EH36 tests indicated that sufficient dynamic effects could be obtained using specimens with relatively small crack lengths (125 mm or greater), a single smaller specimen design (fig. 4) was used for all of the HY80 tests.

PRESENT ANALYTICAL APPROACH

The behavior of the DCB specimens used here should ideally be modeled using dynamic, elastic-plastic fracture mechanics for two reasons: 1. The crack propagation length is sufficiently long that significant wave interaction occurs with the boundaries of the specimen during propagation. 2. The uncracked ligament after arrest reaches net-section yield upon load redistribution. While some preliminary attempts have been made to perform

elastic-plastic modelling of dynamic crack propagation [14], this remains a difficult problem.

Fortunately the experimental results justify significant simplification of the analysis of these tests. The dynamic crack propagation through the weld is accompanied by relatively little plastic deformation. After arrest, the load begins to redistribute and the plastic deformation becomes extensive, but this deformation takes place an order of magnitude more slowly than the elastic straining during crack propagation. Thus, the overall event may be approximately analyzed in two stages: an initial dynamic, linear elastic stage, followed by a quasistatic elastic-plastic stage.

DCB Model

The dynamic linear elastic portion of these tests has been modelled using a modification of Kanninen's model of the DCB specimen, in which the specimen is treated as a Timoshenko beam on a generalized elastic foundation [15]. The modification was made to permit analyzing the effect of the loading spring (ig. 6). The jack was treated as being infinitely stiff, so that displacement is prescribed at the jack point. However, the specimen arm is permitted to pull away away from the jack, in which case the jack load falls to zero. The spring is included at an intermediate point on the beam, and displacement is prescribed on the spring. The mass of the spring and other masses (e.g. the mass of the clevis attached to the spring) are included as a lumped mass between the spring and specimen.

Before performing a dynamic analysis on the actual tests, two checks were made to provide confidence in the model. First, a static analysis of the stress intensity factor was made using the DCB model. This analysis was compared to the predictions of the stress intensity factor from a finite element model of the specimen; the result is shown in figure 7. It is seen that

despite the fact that the arms of the DCB specimen used in the tests reported in this paper are short and deep, Timoshenko beam theory is adequate for modelling them. As an additional check, a dynamic calculation of K as a function of time under specified load was performed using the DCB model. The same analysis was performed using the two-dimensional finite element program reported in [16]. The mesh used in the finite element analysis consisted of constant strain triangle elements and is shown in figure 8. The results for K as a function of time using both models are shown in figure 9. The results of the one dimensional DCB model are considered satisfactory for the time range of interest. The discrepancy between the DCB model calculations and the finite element model results is less than 15% for the first 0.25 milliseconds. The elastic run-arrest portion of all the experiments conducted lasted less than 0.25 milliseconds.

After performing the above checks, the DCB model was used exclusively to model the DCB tests. Only "generation phase" [17] computations were performed, that is, the model was forced to propagate the crack so that the experimentally observed crack growth history a(t) was followed. The value of the stress intensity factor, K, as a function of time was then calculated. The values of jack load and spring displacement measured at initiation were input to the model. Results are presented below in the sections on experimental results.

Plastic Hinge Model

Post-arrest calculations of the J integral and tearing modulus were made using quasi-static elastic-plastic analyses. A simple post net-section-yield model, called the plastic hinge model, for calculating the J integral was derived by assuming that a plastic hinge develops at the uncracked ligament. The derivation is presented in the Appendix; the result is:

$$J = J_e + J_p \tag{5}$$

J_e and J_p are the elastic and plastic parts of J, respectively. J_e is given by:

$$J_e = K^2/E \tag{6}$$

where K is calculated from a static application of the DCB model at the load corresponding to net section yield. Since the specimen arms are relatively long after arrest and this is a static calculation, the simpler Euler-Bernoulli beam model of Kanninen [18] may be used for this purpose. The value of K from this model is [18]:

$$K = [(2\sqrt{3})P/(\lambda B h^{3/2})][\lambda a(\sinh^2\lambda b+\sin^2\lambda b) + \sinh\lambda b\cosh\lambda b-\sin\lambda b\cos\lambda b]/(\sinh^2\lambda b-\sin^2\lambda b) \tag{7}$$

where $\lambda = 6^{1/4}/h$, b = ligament width = W-a and P is the applied load. In evaluating (7), the applied load is set equal to the limit load, P_{limit}, the expression for which is given in the Appendix. Equation (7) is only valid for prismatic beam arms. Therefore, for test EH36-1 a numerical solution for a nonprismatic beam on an elastic foundation was used instead.

From the Appendix, the plastic part of J, J_p, is given by:

$$J_p = \sigma_F[1 + (-2W+2b)\{(2W-b)^2 - b^2\}^{-\frac{1}{2}}](\Delta-\Delta_{NSY}) \tag{8}$$

where Δ is the total deflection at the load point (i.e. on the specimen side of the spring), and Δ_{NSY} is the elastic deflection at the load point evaluated at P_{limit}. This is given by the Euler-Bernoulli DCB model as [18]:

$$\Delta_{NSY} = P_{limit} \times \Theta/EB$$

where

$$\Theta=2(\lambda^3h^3)[2\lambda^3a^3+\{6\lambda^2a^2(\sinh\lambda b\cosh\lambda b+\sin\lambda b\cos\lambda b) +6\lambda a(\sinh^2 b+\sin^2 b) + 3(\sinh\lambda b\cosh\lambda b-\sin\lambda b\cos\lambda b)\}/(\sinh^2\lambda b-\sin^2\lambda b)] \quad (9)$$

For long crack lengths, eq (8) for J_p reduces to the expression for a deeply cracked specimen with remaining ligament in pure bending.

To apply the model for calculating post-arrest J_p in the DCB specimens, the applied load after arrest was first computed quasistatically by accounting for unloading of the spring caused by compliance changes in the specimen during crack propogation. If this calculated applied load, $P_{applied}$, was greater than P_{limit}, it was assumed that plastic deformation of the specimen would occur until the load dropped to P_{limit}. Thus, the value of $\Delta-\Delta_{NSY}$ in eq (8) is given by

$$\Delta-\Delta_{NSY} = (P_{applied} - P_{limit})/K \quad (10)$$

where K is the stiffness of the loading spring. Maximum values of the J integral calculated using this model are shown in Tables I and II for the EH36 tests and HY80 tests, respectively.

The DCB model, of course, does not account for all possible wave modes. Because reflected waves can contribute to crack propagation, the model might be inadequate for a material in which an unaccounted-for wave mode noticeably affected crack propagation. This is not believed to be the case in the present study.

Lumped-Mass Model

A second post-arrest model was developed that accounts for dynamic effects after arrest in a simplified manner. The lumped-mass visco elastic-

plastic model shown in figure 10 was used for this purpose. This model is referred to as the lumped-mass model. All external mass and elastic stiffness of the load train (including those of the loading spring) are included in the parameters M and K. The specimen's mass, M_s, is lumped at a single point. A spring of constant K_s represents the elastic stiffness of the specimen at the load point, a sliding frictional device represents the static limit load of the specimen (the device is rigid when the load applied to it is less than P_{limit} and slides freely when the load reaches P_{limit}), and a dashpot represents the strain-rate elevation of yield stress in the specimen. The applied displacement, elastic specimen crack mouth opening displacement (CMOD), and plastic CMOD are given by U_A, U, and U_p, respectively. within the lumped-mass model, the CMOD and the load point displacement Δ are equal and are given by U. The value of K_s is computed using the static Euler-Bernoulli model for the DCB specimen, eq (7). The dashpot's viscous damping coefficient was computed as follows: A linear relation was assumed to exist between flow strength of the material and strain rate, specifically,

$$\sigma_F(\dot{\varepsilon}) = \sigma_F^0 + c_1\dot{\varepsilon} \tag{11}$$

The value of c_1 was taken to be 0.002/MPa, a typical value for structural steel [5], for both EH36 and HY80. Next, the hinge point in the specimen was found from a static limit-load analysis. Using this hinge point, the crack-tip opening displacement was related to the load-line displacement:

$$CTOD = \Delta d/(W-b+d) \tag{12}$$

where

$$d = .5 \cdot [P_{limit}/(B\sigma_F) + b] \tag{13}$$

is the distance from the crack tip to the hinge point. Finally, an effective "gage length" equal to the specimen thickeness was introduced so that the strain at the crack was approximated by

$$\varepsilon = CTOD/B \tag{14}$$

Using (11-14), the result for the dashpot coefficient is

$$C_s = (c_1 dP_{limit})/(\sigma_F(W-b+d)) \tag{15}$$

The differential equations governing the two degree-of-freedom system in figure 10 are

$$(K+K_s)\,U + M\ddot{U} - K_s U_p = KU_a \tag{16}$$

$$K_s(U-u_p) - C_s\dot{U}_p - M_s\ddot{U}_p = P_{limit} \tag{17}$$

When the load in the specimen does not exceed the static limit load, eqs (16) and (17) reduce to the single expression

$$(K + K_s)U + M\ddot{U} = KU_A \tag{18}$$

When the model is used solely for post-arrest calculations with a stationary crack, then (16-18) are linear and may be solved in closed form. When a running crack is analyzed, K_s, P_{limit}, and C_s, depend inplicitly on time in a complicated, nonlinear fashion, and the model must be solved numerically. After solving (16-18), the J integral as a function of time can be calculated. The plastic displacement, U_p, from the lumped-mass model is equal to $\Delta-\Delta_{NSY}$ in eq (8), thus J_p can easily be calculated. Given U(t) and $U_p(t)$, the elastic force,

P, acting on the specimen can be calculated, and J_e can be evaluated using eqs (6,7).

Dynamic effects in the lumped-mass model are too simplified to properly represent the elastic run-arrest portion of the tests. For example, wave motion along the specimen arms (which act as waveguides) is not present in the lumped-mass model. For this reason, for modeling the pre-arrest portion of a test, where the details of dynamic effects are more important but plasticity is negligible, the one-dimensional Kanninen model was used. Calculations with this model were carried out until the instant of arrest. The solution to the Kanninen model at the time of arrest permitted the calculation of U and $\dot{U}$, to be used as initial conditions for the lumped-mass model. (The initial values of U_p and $\dot{U}_p$ are zero because at the instant of arrest the specimen has not yielded.)

In addition to permitting estimates for the post-arrest J integral, the lumped-mass model is attractive because it qualitatively represents the situation in a ship: The external mass and external stiffness, M and K, represent the "effective global mass" and "global stiffness" of the structure, while all other parameters represent the cracked section of the structure.

As will be seen in table II, below, the J-integral values calculated using these approximations high, on the order of 2 MN/m (11,000 lb/in). These high values are hard to believe, and so the simplified analytical procedure outlined above must be questioned. In Results and Discussion below, results calculated according to the present procedure will be listed. Other results, calculated using a different version of the lumped-mass model, will be given also. These results will show that J rises rapidly with time during the crack arrest-reinitiation time period. This implies that obtaining correct crack length values for correlation with J values to form a dynamic J-R curve may be

difficult. The other results will also allow an estimate of the degree of uncertainty present in these calculations of dynamic J during the crack arrest-reinitiation event, which are believed to be the first such calculations ever reported.

Post-Arrest Tearing Modulus

A static post-arrest calculation was used to estimate the applied tearing modulus, T_{app} for this specimen. The procedure presented in Appendix I of ref. [19] was used to derive an expression for a deeply-cracked double cantilever beam specimen under spring loading. The result is:

$$T_{app} = 2b^2(2W-b)/h^3+(EB/K)(1+(2b-2W)/[(2W-b)^2+b^2]^{\frac{1}{2}})b/(2W-b) \qquad (19)$$

where b is the uncracked ligament width after arrest.

MATERIALS

Crack arrest tests were performed on two steels: EH36 and HY80. The tests of EH36 were used to refine the experimental procedures; HY80 was tested because it is used as a crack arrester material in ships.

EH36 is a tough carbon-manganese steel used in ships and other large engineering structures. Its flow strength, increases from about 430 MPa to about 520 MPa as temperature decreases from 0 to -70°C. It has a sharp ductile-brittle transition at around -75°C, Fig. 11.

HY80 is a low carbon, nickel-chromium-molybdenum alloy steel with excellent toughness and ductility. Its flow strength at 0°C is about 670 MPa, rising to about 750 MPa at -100°C. Its nil-ductility temperature is in the range -60 to -100°C. Its room temperature static tearing modulus, for crack extensions of the order of 1 mm, is about 70.

EXPERIMENTAL PROCEDURES AND RESULTS

The EH36 specimen material was used to develop experimental procedures, which were then applied to HY80. Therefore, the procedures and results for these two specimen materials will be discussed separately.

Experimental Procedure-EH36 Specimens

A ductile-to-brittle transition curve obtained from Charpy tests [20] for EH36 steel is shown in figure 11. Before testing the crack arrest specimens, static fracture toughness testing was performed on the electron beam welds. A plate of EH36 base metal was electron beam welded with the weld parallel to the rolling direction. Three point notched bend bars, 25 mm square, were cut from the specimen with the notch oriented so that crack growth would be in the plane of the plate (fig. 12). A starter notch of approximately 10 mm in length was cut and then fatigue sharpened to 12 mm. Five specimens were tested at temperatures ranging from -40 to -100°C. The lower shelf of the material was reached at approximately -50°C, and the lower shelf toughness was approximately 80 MPa$\sqrt{M}$.

This toughness value was used to estimate the starter notch length required in the specimens. The relation between applied load and K was calculated as discussed above in the analysis section. Starter notches were sawed into the specimens approximately 5 mm shorter than the desired length, and the notches were then fatique sharpened to reach the final length. Fatiguing was performed in a 980 kN servo-hydraulic testing machine at 5 Hz. Typically 20,000 cycles were required. Fatigue crack growth rates were slower than expected for the ΔK levels applied. This was due to the presence of compressive residual stress in the crack arrest specimens. For the same reason higher than expected loads were typically needed to cause initiation of unstable crack propagation. The residual stress was estimated to effectively

reduce the applied value of K by approximately 40 Mpa$\sqrt{m}$. After this effect was discovered it was offset by increasing the final fatigued notch length by approximately 20 mm. The starter crack lengths used in each of the tests are shown in figure 5.

Cooling of the specimens was performed using a box, made of polystyrene foam in which copper cooling coils were placed. The coils were in contact with the specimen over a large region; liquid nitrogen was cycled through them. In addition, liquid nitrogen was injected against the specimen at the starter-notch tip. The goal was to achieve a low enough temperature at the notch tip to assure lower shelf behavior of the weld, while maintaining the desired test temperature in the remainder of the specimen. Nylon pins were used during cooling to reduce the heat sink effect of the clevis grips. These were replaced by steel pins before loading.

In the first test a specimen temperature of 0°C was used. This was intended to assure upper shelf behavior of the base metal at the instant the crack propagated to the end of the weld. The test temperature in the second test was -70°C. This test was intended to show that arrest would not occur in the specimen if the arrest material were brought sufficiently down from the upper shelf. The third specimen was tested at 0°C. Arrest was intended to occur in this test as in the first test. However, as discussed above under specimen design, the uncracked ligament width of the specimen was chosen so that severe ductile tearing of the ligament would occur upon load redistribution.

After cooling the specimens to the desired temperature, a main load of 410 kN was applied through the loading spring shown in figure 3. The starter notch length was chosen such that unstable crack propagation should occur at this load level. However, because of scatter in initiation toughness values

and the residual stress effect mentioned above, typically higher K values were needed than that corresponding to 410 kN. The loading jack was then used to apply additional load until the specimen failed. In the third test on EH36, a large ratio of jack load to main load was needed (main load 410 kN, jack load 160 kN). The stiffer jack tended to make the fracture process more stable, which caused a pop-in of approximately 5 mm in length to occur in this test. The jack load was then reapplied and unstable crack propagation took place at a jack load of 180 kN.

Experimental Results For EH36 Steel

In the first experiment the temperature in the arrest section of the specimen was approximately 0°C. Dynamic crack propagation occurred until the end of the electron beam weld was reached where upon the crack arrested abruptly. In the second experiment the arrest material was at -70°C. Referring to figure 11, this material has a very sharp ductile-brittle transition at approximately -70°C. In this test arrest did not occur. In the last test the ligament width had been chosen so that after arrest the net section yield load was exceeded. This caused a significant amount of stable ductile tearing to occur.

Transient data are shown for the first and third tests in figures 13-15. Due to a power supply failure the transient data were lost in the second test. Crack length as a function of time for the first test is shown in figures 13a. The crack tip quickly accelerated to a speed of approximately 750 m/sec and propagated at this speed for 120 microseconds until the end of the weld, after which arrest occurred abruptly. Applied load as a function of time for this test is shown in figure 14. A load drop of approximately 16% occurred during crack propagation. After arrest, the load dropped further and then recovered.

Strain gages were placed near the end of the weld at the location shown in Fig. 4. These were intended to be in the point of the slip-band pattern for studying the evolution of plastic deformation. The trace from the strain gage farther from the end of the weld was lost. Strain in the near gage as a function of time is shown in Fig. 15. The strain at this point increased rapidly but remained below yield until after arrest. After arrest, upon load return (Fig. 14) yield occurred. The plastic deformation increased at a rate approximately an order of magnitude smaller than the elastic strain rate during the crack run. This experimental observation, which was repeated in the third test, is felt to justify the analytical approach presented above: the dynamic crack propagation event was accompanied by relatively little plastic deformation but occurred rapidly, and so it can be treated by dynamic LEFM analysis; the post-arrest deformation and reinitiation involved extensive plastic strain, but developed slowly, and so can be treated by quasi-static EPFM analysis.

The plots of the stress intensity factor, K, as a function of time inferred from the crack speed data using the DCB model described in the analysis section are shown in Fig. 16. It is seen that the stress intensity factor remained above K_{IC} for EH36 during both tests. Because the crack propagation toughness, $K_{ID}(\dot{a})$, should be lower than K_{IC}, the static-initiation toughness, arrest did not occur because of load drop but instead occurred because the step in toughness at the end of the weld was encountered. The dynamic K values at the instant the end of the weld was encountered, given in Table 1, were obtained from the plots of Fig. 16, by using the trip wire data to get the time at which the crack encountered the end of the weld.

Crack length as a function of time for the third test is shown in Fig. 13b. In this test the crack tip reached a high speed of approximately

1,000 m/s during the early stage of crack propagation but decelerated to 167 m/s prior to arrest. The applied load as a function of time is shown in Fig. 14b. In this more massive specimen a larger compliance change occurred during crack propagation so load drop was more severe. The load had dropped approximately 45% at arrest. The value of stress intensity K as a function of time calculated using the DCB model is shown in figure 16b. The stress intensity factor remained above K_{IC} throughout crack propagation, so that arrest would not have occurred without the step in toughness at the end of the weld. However, because of the relation between $\dot{a}$ and applied K the crack did decelerate considerably during crack propagation. Strain in the vicinity of the end of the weld as a function of time for the nearer-tip location shown in figure 4 is plotted in figure 15b. As for the first test it is seen that rapid elastic straining of this region took place during crack propagation, followed by more slowly developing plastic deformation after arrest.

The crack propagation gages indicated that reinitiation occurred during the third test. The last gage was placed in the base metal approximately 5 mm from the end of the weld. The next to last gage was located 12.5 mm from this gage. An interval of 1.5 m occurred between the breaking of the next to last and last gages indicating arrest followed by reinitiation. From examining the fracture surfaces it appears that approximately 40 mm of stable tearing occurred after reinitiation. Using the plastic hinge model, the quasistatically calculated value of the J integral was 0.86 kN/m in this specimen. The upper shelf value of the static-initiation toughness, J_c, is approximately 0.3 kN/m [20] for this material so tearing was expected. As discussed above, the applied tearing modulus did not exceed T_{mat} so unstable tearing did not occur.

For the specimen in which reinitiation occurred (test EH36-3), the tearing modulus was calculated statically using eq(19) with the result

T_{app}=37. Based on results for a similar C-Mn steel [21], this is less than the tearing modulus, T_{mat}, for EH 36, which should be greater than 50, so unstable tearing was not expected, and, in fact, did not occur.

The series of tests on EH36 permitted development of the test method. It was demonstrated that, using the modified DCB specimen design, arrest does not occur if the material is not tough enough to force a fracture mode change from cleavage to tearing, but does occur if it is, and that reinitiation in ductile metal is possible upon load redistribution to the uncracked ligament.

Experimental Procedure- HY80 Specimens

As discussed in the section on EH36 specimens, before testing the specimens of HY80, the fracture toughness of the electron-beam weld in HY80 was first measured using static three-point bend bar tests. Five specimens were tested at temperatures ranging from -20°C to -50°C. The lower shelf temperature of the weld material was approximately -50°C, and the lower shelf toughness was (formally invalid, indicated by subscript q) K_q = 70 Mpa$\sqrt{m}$. The starter notch lengths in the DCB specimens were chosen so that the initiation toughness should be reached at a load of 410 kN in the loading spring with no jack load. The entire jack load was then available as reserve. To account for the residual stress effects in the electron-beam weld in the DCB specimen, the starter notch length was increased slightly, to 55 mm, for each of the HY80 specimens. The notches were saw cut with a root radius of approximately 0.11 mm. Fatigue pre-cracking was not used in the HY80 tests for two reasons: 1) Using a blunt starter notch permits the initiation toughness, K_q, to exceed K_c, so that the crack has more of a tendency to propagate unstably [22]. 2) In the EH36 specimens it was found that the fatigue cracks had a tendency to turn out of the weld.

Cooling of the specimens was accomplished using the device discussed in the section on EH36. The main load of 410 kN was then applied through the

loading springs. If this load was insufficient to cause initiation, the main load was then supplemented with the jack load.

Experimental Results-HY80 Specimens

The experimental results are summarized in Table II and described and discussed in detail below. The first test was a failure because an insufficiently high energy electron-beam weld was used. The weld was not brittle enough and the crack turned out of the weld before the end of the weld was encountered. This was remedied by locating a higher energy electron-beam welder (50 KV, 170 mA), capable of welding the 25 mm thick specimens in one pass. In all subsequent tests the crack ran straight along the weld until the end of the weld was encountered. The highest temperature at which arrest first failed to occur because the crack ran straight into the HY80 in cleavage was found to be -70±10°C. This falls in the range of nil-ductility temperatures reported for HY80, approximately -60 to -100 C [23].

The stress intensity, K, values reported in column 5 of Table II, for the instant the running crack encountered the end of the weld, do not represent specific values of crack arrest toughness for HY80. It is claimed that, for those specimens in which arrest was observed, the crack arrest toughness must have been higher than the K value at which arrest actually occurred (specimens HY80-2, and 4-7). For the specimens in which arrest did not occur, the crack arrest toughness must have been lower than the K value used (specimens HY80-3 and 8).

In tests HY80-2, HY80-4, and HY80-5 the fracture mode changed from cleavage to tearing and arrest occurred at least momentarily. Reinitiation in ductile tearing then occurred in each of these tests. The pause time between arrest and reinitiation was typically approximately 1.5 m, or an order magnitude longer then the initial run-arrest time. Typical fracture surfaces

are shown in Fig. 17. In test HY80-2 the reinitiation was stable and a ductile tearing "thumbnail" of approximately 40 mm in length appears on the fracture surface. In tests HY80-4 and HY80-5 the reinitiation was stable at first, but became unstable after 40-50 mm of tearing. The unstable tearing was in a macroscopic tearing (shear lip) mode. Thus the tearing modulus of HY80 appears to be strongly temperature-dependent in this temperature range.

Tests HY80-2, HY80-7, and HY80-8 form another series. By varying the number of washers the applied tearing modulus was varied from approximately 28 to 53. At -35°C HY80 is on the upper shelf so the material resistance to tearing is the same as at room temperature. Room temperature J integral resistance curve data for HY80 were reported in Ref. [24]. The tearing modulus is initially approximately 100, but, because of the "roundhouse" nature of the resistance curve, drops off to approximately 40 after several millimeters of tearing. In each of tests HY80-2, HY80-7, and HY80-8 at least 40 mm of stable tearing occurred. In tests HY80-7 and HY80-8 this was followed by instability in the shear lip mode. From these results, it was concluded that the tearing modulus of HY80 on the upper shelf under the dynamic conditions of these modified DCB tests is approximately 35 ± 6. The driving force values reported in Table II were inferred from the test parameters by using the models discussed in the analysis section.

Detailed plots of the data recorded in each of the HY80 tests are shown in Figs. 18 to 20. The plots of crack position as a function of time, Figs. 18a-f, show that typically the crack ran at high speed (on the order of 500 m/s) through the weld. In tests HY80-3 and HY80-8 the crack did not arrest. The transient data was lost from test 8 because a slight pop-in immediately prior to initiation caused premature triggerring. The plot from test HY80-3 (Fig. 18b) shows that the crack continued at high speed past the end of the

weld. In each of the tests in which arrest occurred (HY80-2,4,5,6, and 7) a pause of approximately 1.5 ms is evident in between the time at which the last crack gage across the weld was broken and the first gage in the base metal (approximately 5 mm from the end of the weld) was broken. In tests HY80-7 and HY80-8 in which unstable reinitiation occurred, the crack speed in the tearing mode varied from 5 to 30 m/s.

The plots of load as a function of time are similar for each of the tests. From Fig. 19 it is evident that a relatively small amount of load drop occurred up to the instant of arrest. The load then dropped precipitously as the beam arms in the specimen continued to move apart at a high speed while the mass of the loading spring prevented immediate load recovery. The load then recovered after approximately 1-2 ms. The period of the oscillations in the load trace corresponds to the transit time of a wave along the beam arms from the crack tip to the loading point and back.

In test HY80-2, a strain gage was placed in the vicinity of the end of the weld along the slip-band path (Fig. 20) and shows fast elastic straining up to instant of arrest, followed by yielding and slower plastic deformation as the load returns and is distributed to the uncracked ligament.

Using the initial applied load and the crack growth history as input, the modified DCB model was used to calculate K as a function of time prior to arrest (Fig. 21a-f). The dynamic K values at the instant the weld was encountered, given in Table II, were obtained from the plots of Figs. 21a-f, by using the trip-wire data to get the time at which the crack encountered the end of the weld.

Load-line displacement and velocity at the instant of arrest were used as initial conditions to predict J as a function of time up until the instant of

reinitiation, using the lumped-mass viscoelastic-plastic model discussed above; the results for J at the instant of reinitiation are also shown in Table II.

Application of the J-integral to dynamic crack reinitiation in crack arrest tests constitutes an extension of the J-integral beyond its known range ov validity and into a range where even its correct definition is unknown. Another report [26] examines the definition and evaluation of fracture mechanics parameters in crack arrest tests. In that report, a different implementation of the lumped-mass model described above was used to calculate J as a function of time after arrest. The results for two specimens are shown in Figs. 22 and 23. The time axis on these figures corresponds to the oscilloscope time reference. Re-initiation is believed to have occurred in both these tests at about 1.5 ms. These results indicate that J at reinitiation was in the range 0.4 to 0.8 MN/m, more than twice the room-temperature static J_{Ic} value but less than the values given in Table II. But the plots clearly show that small errors in the reinitiation time could lead to large errors in J at reinitiation.

It is believed that the J levels at reinitiation are larger than the static J_{Ic} values, by an unknown amount. The present uncertainty in J should be attacked by seeking a proper definition of J applicable to both specimens and structures, by searching for accurate methods to evaluate J, and by attempting to make use of all existing data and to get better data in future tests.

CONCLUSIONS

A new test method has been devised to simulate conditions under which cracks propagate long distances and arrest at high toughness interfaces in ships. Results on EH36 ship steel and HY80 were described. Successful crack arrest in these experiments, when it occurred, consisted of two phases;

1) Arrest occurred when the crack encountered the step in toughness between the brittle weld and the arrester material. The arrest material was on the upper shelf and had sufficient toughness to force a fracture mode transition; In the tests in which this condition was not met, because the arrest material was below its ductile/brittle transtion temperature, arrest did not occur. 2) After arrest the loading spring reloaded the uncracked ligament causing severe plastic straining. The arrest material had a sufficiently high tearing modulus to prevent reinitiation in unstable tearing. In the test in which this condition was not met, because of high loading system compliance, unstable tearing followed by specimen failure occurred.

Both of the above phases are believed to be present in the run-arrest event in ship structures. The first phase is addressed by existing tests, such as the hybrid double tension test [12], but the second phase is not.

In the HY80 series of tests it was possible to use the test method to quantitatively evaluate the arrest performance of a steel under conditions simulating those in a ship. It was found that the temperature below which a fracture mode transition from cleavage to tearing will not occur is approximately -70°C. This value provides a valuable basis for comparison of the arrest performance of other steels to HY80. In addition, it was found that the value of applied tearing modulus at service temperature above which the arrester steel was unable to prevent failure by unstable reinitiation in tearing was approximately 34.

This test method provides the basis for quantitative materials selection criteria for the crack-arrester strake application. It can be applied in two manners: 1) The relative performance of candidate steels for the arrester application can be assessed. For this purpose the results already obtained on HY80 steel will serve as a useful comparison. 2) The

absolute suitability of a steel for the arrester application in a specific ship can be determined. The test method described qualitatively simulates conditions in a ship. To make the simulation quantitative will necessitate proper choice of the experimental parameters: the loading spring and total external mass must properly represent the "global" compliance and inertia of a ship, while specimen parameters (specimen size, crack jump length, ligament width) represent "local" conditions in the cracked section of a ship. These parameters can only be chosen properly by using analytical modeling of hypothetical run-arrest events in specific ships.

Appendix: Static J Integral Solution for DCB Specimen After Net Section Yield

Following the approach of Rice, Paris and Merkle [25], the J integral after net section yield is expressed as a sum of elastic and plastic parts:

$$J = J_e + J_p \tag{20}$$

The elastic part is determined from a stress intensity factor solution. The Kanninen beam-on-elastic foundation model was used for this purpose as described in the text. The plastic part is derived from a plastic hinge analysis:

$$J_p = -(1/B) \int_{\Delta_{NSY}}^{\Delta} \frac{\partial P}{\partial a} \, d\Delta \tag{21}$$

where P is the load applied to the specimen, B is specimen thickness, and Δ is the load-point deflection. The material is assured to be perfectly plastic, and after net section yield P is equal to P_{limit}. Equation (21) then reduces to

$$J_p = -(1/B)\partial P_{limit}/\partial a \, (\Delta - \Delta_{NSY}) \tag{22}$$

P_{limit} is determined by assuming that a plastic hinge has developed at the cracked section, and is given by

$$P_{limit} = B\sigma_F \left[-(2W-b) + \{(2W-b)^2 + b^2\}^{\frac{1}{2}}\right] \tag{23}$$

where W is the total width of the specimen measured from the load line to the end and b is the uncracked ligament width.

By differentiation, one obtains:

$$\partial P_{limit}/\partial a = -\sigma_F[1+(-2W+2b)\{(2W-b)^2+b^2\}^{-\frac{1}{2}}] \qquad (24)$$

Substituting (24) into (22), the expression for J_p presented in the text (Eq.8) is obtained.

ACKNOWLEDGMENT

The authors would like to express their appreciation to David McColskey, Daniel Vigliotti and John Moulder for valuable assistance in performing the experiments described in this paper.

This report was prepared as part of the Fracture Control Technolgy Program under the sponsorship of Dr. H. H. Vanderveldt, Naval Sea Systems Command (SEA 05R25). The effort was directed by Mr. John P. Gudas, David Taylor Naval Ship R&D Center, under Program Element 62761N, Task Area Sf-61-544-504.

REFERENCES

1. R. B. King, "Interim Progress Report: Materials Selection Criteria For Crack Arrester Strakes in Naval Vessels", NBSIR 83-1681, Jan. 1983.

2. Hahn, G. T., Rosenfield, A. R., Marshall, C. W., Hoagland, R. G., Gehler, P. C., and Kanninen, M. F., "Crack Arrest Concepts and Applications", in Fracture Mechanics, eds N. Perrone et. al., University of Virginia Press, Charlottesville, Va., 1978, pp. 205-227.

3. Hoagland, R. G., Rosenfield, A. R., and Hahn, G. T., "Mechanisms of Fast Fracture and Arrest in Steels", Met. Trans., V. 3, 1972, pp. 123-136.

4. Ogura, N., "A study on the Ductile Arrest of a Brittle Crack", J. Soc. Naval Arch. Japan, V.110,1961, pp. 443-453.

5. Krafft, J. M., and Irwin, G. P., "Crack Velocity Considerations", Fracture Toughness Testing and Its Applications, STP 381, ASTM, Philadelphia, Pa., 1965, pp. 114-129.

6. Freund, L. B., "Dynamic Crack Propagation", The Mechanics of Fracture , ed. F. Erdogan, ASME AMD, V. 19, ASME, N. Y., 1975, pp. 105-134.

7. Kihara, H., Kanazawa, T., Ikeda, K., Okage, H., Nakajima, T., and Lajima, A., Study on Welded Type Crack Arrester, IIW Doc. No. X-618-71, 1971.

8. Kanazawa, T., Machida, S., and Teramoto, T. "Study on Fast Fracture and Crack Arrest", Exp. Mech., V. 21, 1981, pp. 78-88.

9. Freund, L. B., private communication.

10. Hutchinson, J. W., and Paris, P. C., "Stability Analysis of J-Controlled Crack Growth", Elastic-Plastic Fracture, ASTM STP 668, J. D. Landes, J. A. Begley, and G. A. Clarke, Eds, ASTM, Philadelphia, Pa., 1979, pp. 37-64.

11. Kawaguchi, Y., Tsukamoto, M., Maruyama, K., Bessyo, K., and Kato, Y.,"Crack Arrestability of Ni Steel Plates for Low Temperature Service to the Extremely Long Brittle Crack", in Proceedings, International Conference on Fracture Toughness Testing, the Welding Institute, Cambridge, U. K., 1982.

12. Machida, S., Kawaguchi, Y., and Tsukamoto, M., "An Evaluation of the Crack Arrestability of 9 % Ni Steel Plate to an Extremely Long Brittle Crack", J. Soc. Nav. Arch. Japan, V. 150, 1981, pp. 569-575 (in Japanese).

13. Green, A. P., and Hundy, B. B., "Initial Plastic Yielding in Notched Bend Tests", J. Mech. Phys. Solids, V. 4, 1956, pp. 128-144.

14. Dahlberg, L., "Plastic Effects in Dynamic Crack Propagation", Advances in Fracture Research, Proceedings of the Fifth International Conference on Fracture, Pergamon, Oxford, 1981, pp. 2195-2203.

15. Kanninen, M. F., "A Dynamic Analysis of Unstable Crack Propagation and Arrest in the DCB Test Specimen", Int. J. Fract., V. 10, 1973, pp. 415-430.

16. Malluck, J. F., and King, W. W., "Fast Fracture Simulated By Conventional Finite Elements: A Comparison of Two Energy-Release Rate Algorithms", Crack Arrest Methodology and Applications, ASTM STP 711, G. T. Hahn and M. F. Kanninen, eds., ASTM, Philadelphia, Pa., 1980, pp. 38-53.

17. Kanninen, M. F., "Critical Appraisal of Solution Techniques in Dynamic Fracture Mechanics", Numerical Methods in Fracture Mechanics, eds. A. Luxmoore and R. Owen, University of Swansea Press, Swansea, U. K., 1978, pp. 612-633.

18. Kanninen, M. F., "An Augmented Double Cantilever Beam Model for Studying Crack Propagation and Arrest", Int. J. Fract., V. 9, 1973, pp. 83-91.

19. Paris, P. C., Tada, H., Zahoor, A., and Ernst, H., "The Theory of Instability of the Tearing Mode of Elastic-Plastic Crack Growth", Elastic-Plastic Fracture, ASTM STP 668, J. D. Landes, J. A. Begley, and G.A. Clarke, eds., ASTM, Philadelphia, Pa., 1979, pp. 5-36.

20. Anderson, T., and McHenry, H. I., "Fracture Toughness of Steel Weldments for Arctic Structures", NBSIR 83-1680, Jan. 1983.

21. Pitman, S. "An Investigation of the Toughness Transition of a C-Mn-Cb Steel for Static and Dynamic Loading", Master's Thesis, Colorado School of Mines, 1978.

22. Hahn, G. T., Hoagland, R. G., Kanninen, M. F., Rosenfield, A. R., and Sejnoha, R., "Fast Fracture Resistance and Crack Arrest in Structural Steels", Ships Structures Committee Rept. No. SSC-242, 1973.

23. Babecki, A. J., and Puzak, P. D., "Explosion Test Performance of Small-scale Submarine Hull Weldments", NRL Memo Rep. 996, 1959.

24. Vasilaros, M. G., Gudas, J. P., and Joyce, J.A., "Experimental Evaluation of Tearing Instability Phenomena for Structural Materials", Rept. No. NURGE/CR-2570, U.S. Nuclear Regulatory Commission, Washington, DC, 1982.

25. Rice, J. R., Paris, P. C., and Merkle, J. G., "Some Further Results of J-Integral Analysis and Estimates", Progress in Flaw Growth and Fracture Toughness Testing, ASTM STP 536, ASTM, Philadelphia, Pa., 1973, pp. 231-245.

26. Teramoto, T., Read, D. T., and King, R. B., "Fracture Mechanics Parameters in Crack Arrest Specimens," NBSIR, to be published.

TABLE I Results for tests of EH36 steel

Specimen	Temperature (°C)	Number of Springs	K at initiation (MPa√M)	K at instant end of weld was encountered (MPa√M)	Arrest	Reinitiation Amount of Tearing	Maximum J before reinitiation (Static Calculation)	Tapp
EH36-1	0	8	120	84	yes	no	0.24	--
EH36-2	-70	8	132	92	no	--	--	--
EH36-3	0	8	177	89	yes	yes 25mm	0.86	37

TABLE II Results for tests of HY80 steel.

Specimen	Temperature (°C)	Number of Springs	K at initiation (MPa√M)	K at instant end of weld was encountered (MPa√M)	Arrest	Reinitiation Amount of Tearing	Maximum J before reinitiation (static calculation) MN/m	J at instant of reinitiation (dynamic calcualtion) MN/m	Tapp
HY80-2	-35	8	154	139	yes	yes 40 mm	2.2	1.82	24.8
HY80-3	-100	8	104	78	no	--	--	--	--
HY80-4	-50	16	130	104	yes	yes unstable	2.2	2.36	24.8
HY80-5	-35	16	114	97	yes	yes unstable	3.48	2.78	46.4
HY80-6	-35	12	108	103	yes	yes unstable	2.31	2.08	35.6
HY80-7	-60	8	158	119	yes	yes unstable	2.2	1.64	24.8
HY80-8	-80	8	198	148	no	--	--	--	--

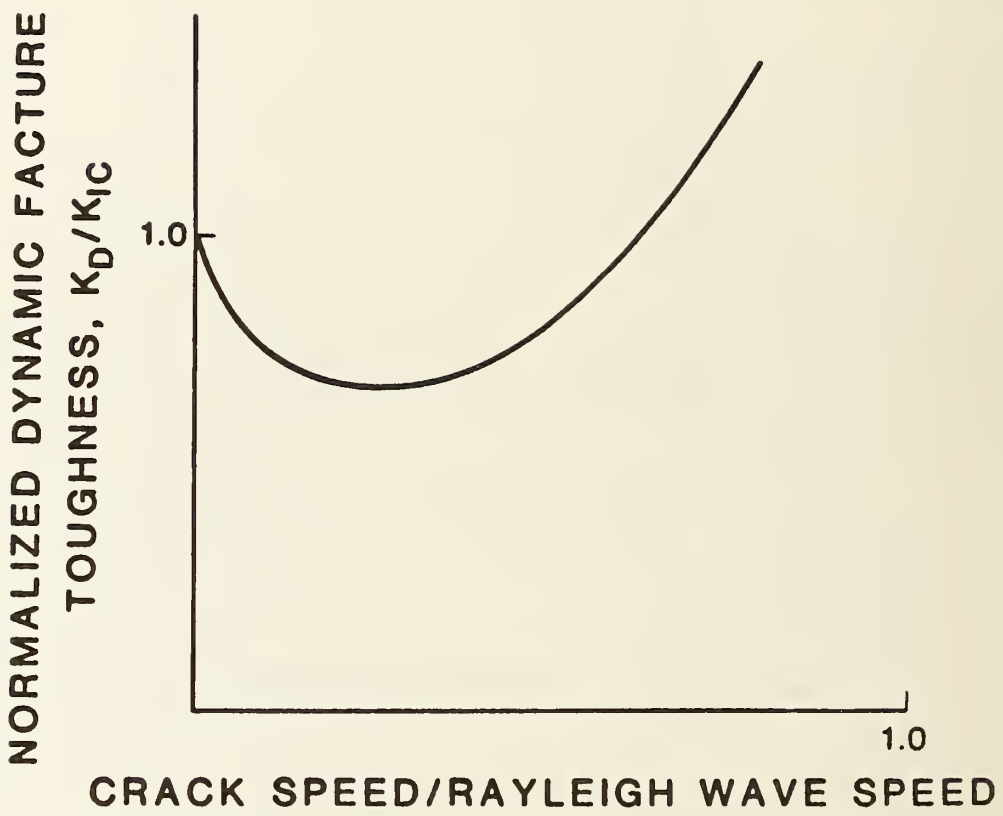

Figure 1. Schematic plot of K_D as function of å.

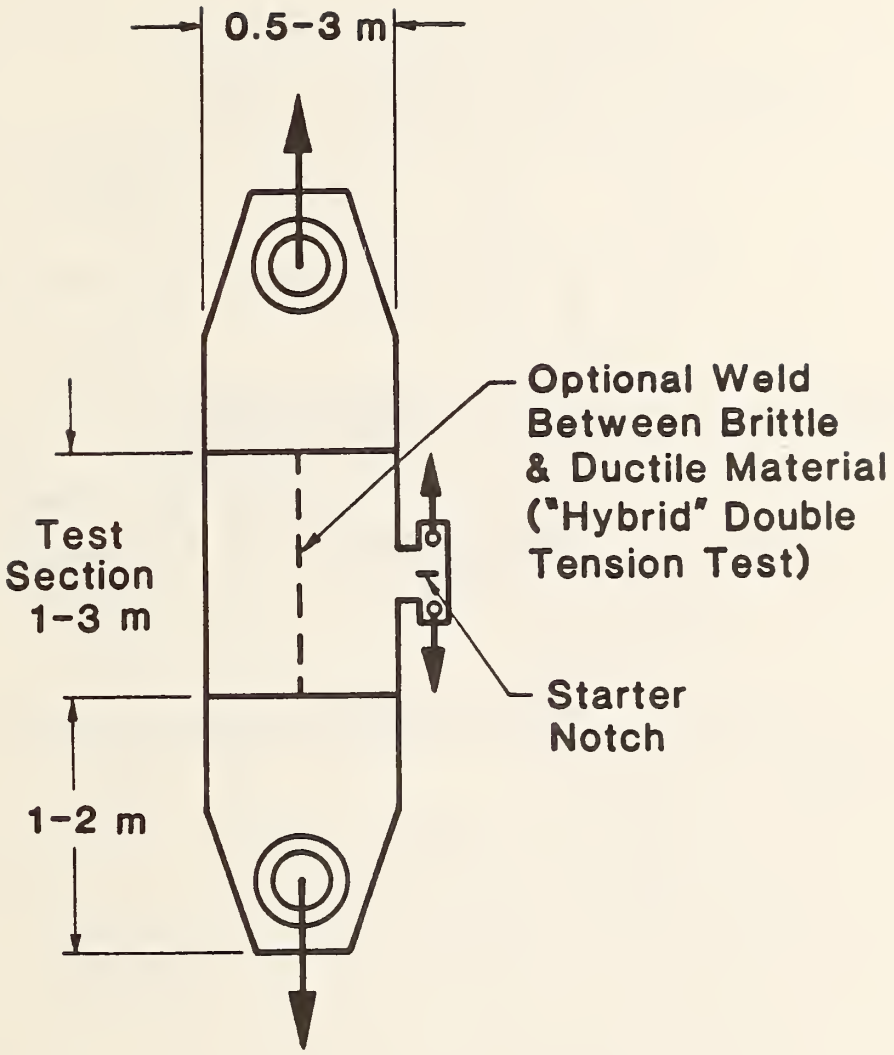

Figure 2. Double-tension specimen.

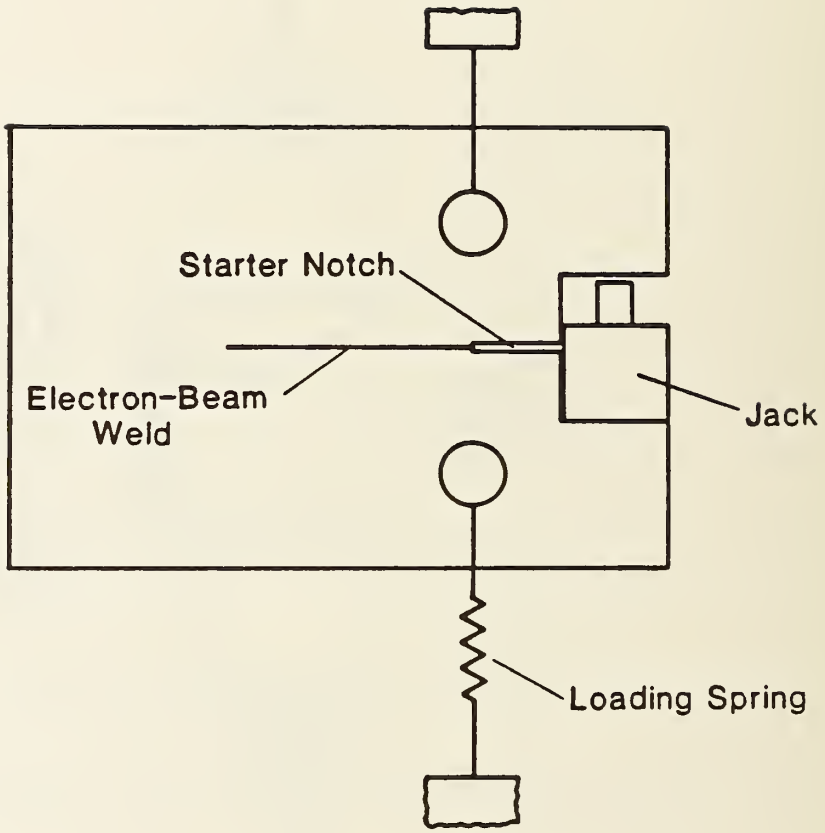

Figure 3. Modified double-cantilever beam specimen.

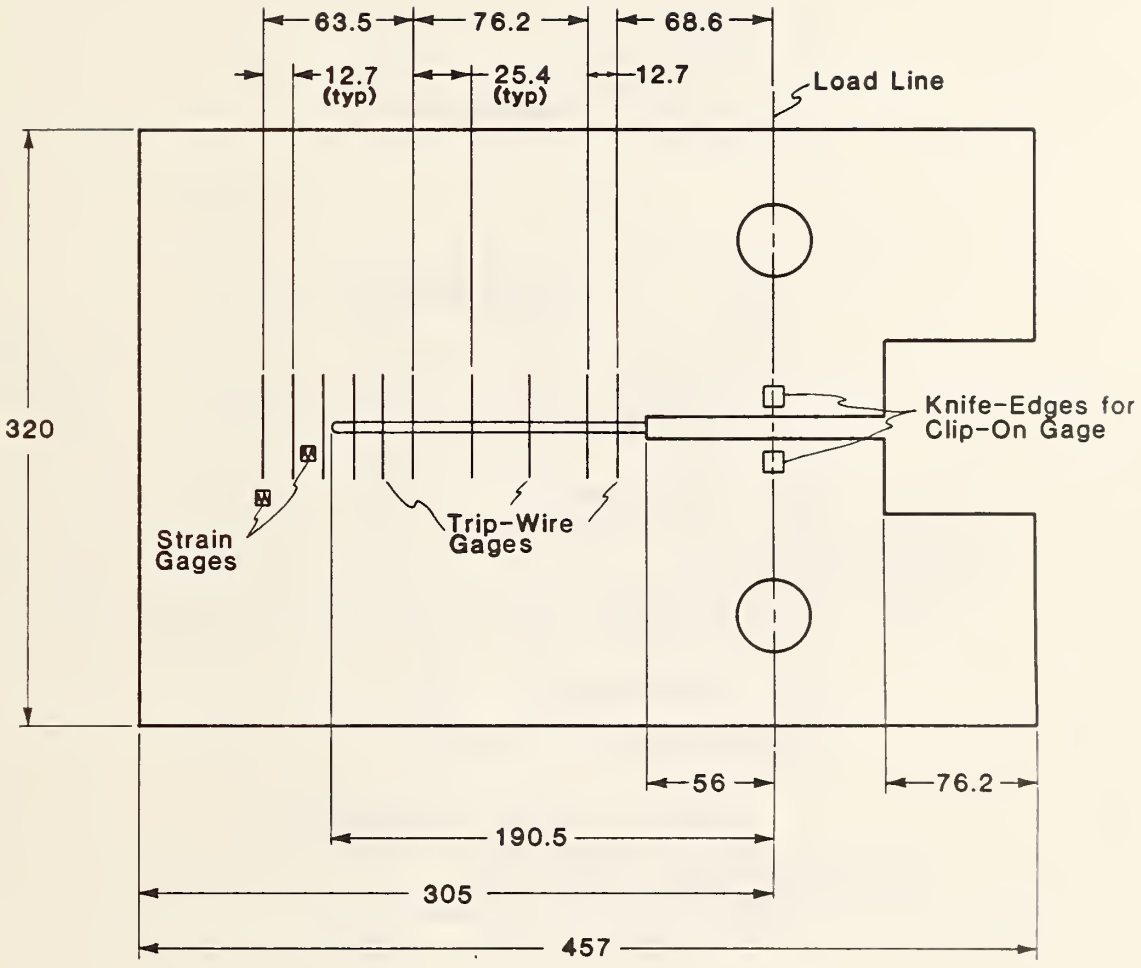

Figure 4. DCB Specimen used for HY80 tests.

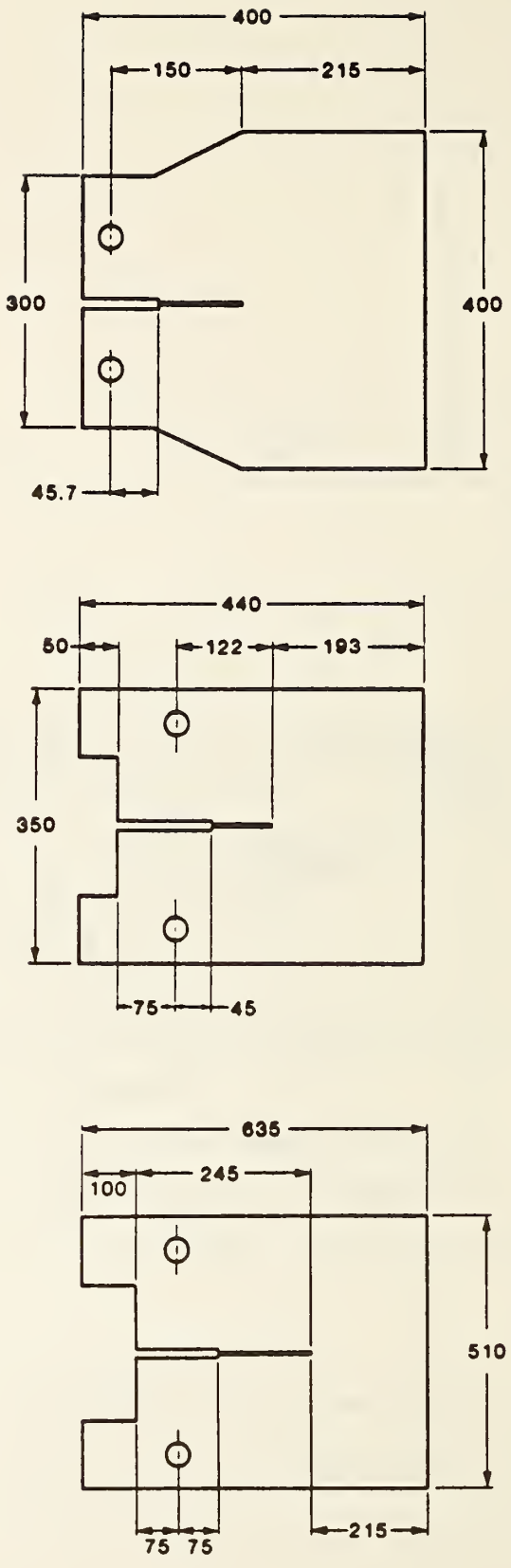

Figure 5. DCB Specimen dimensions for EH36 tests.

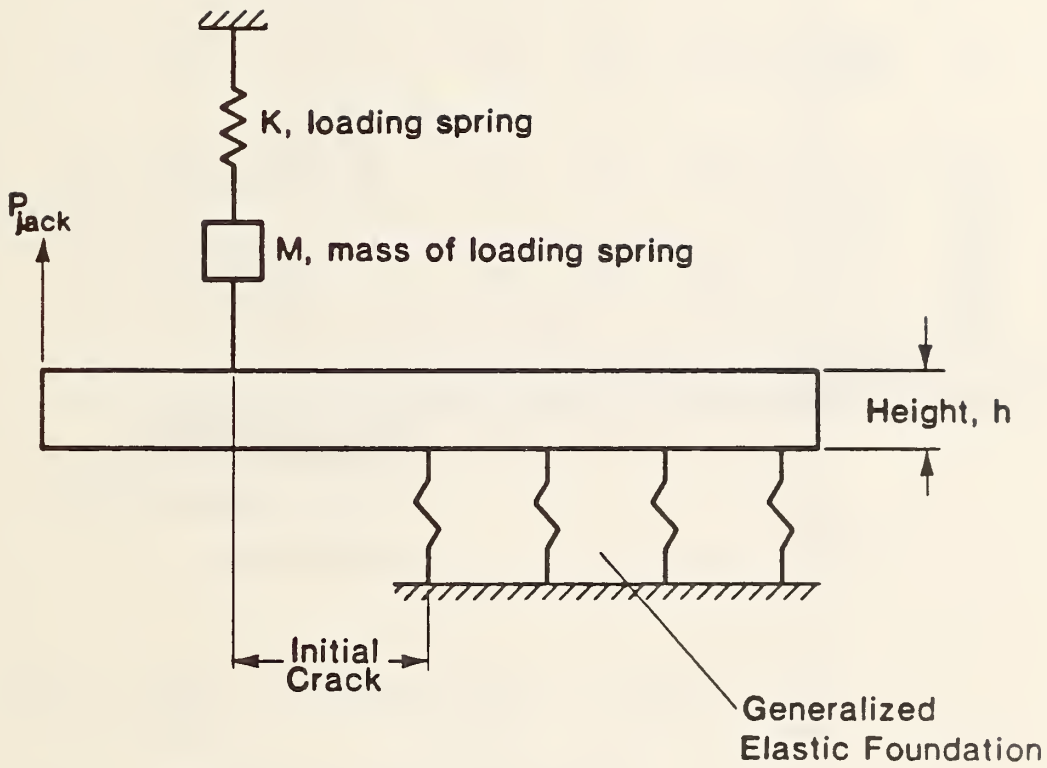

Figure 6. Modified one-dimensional model for DCB specimen.

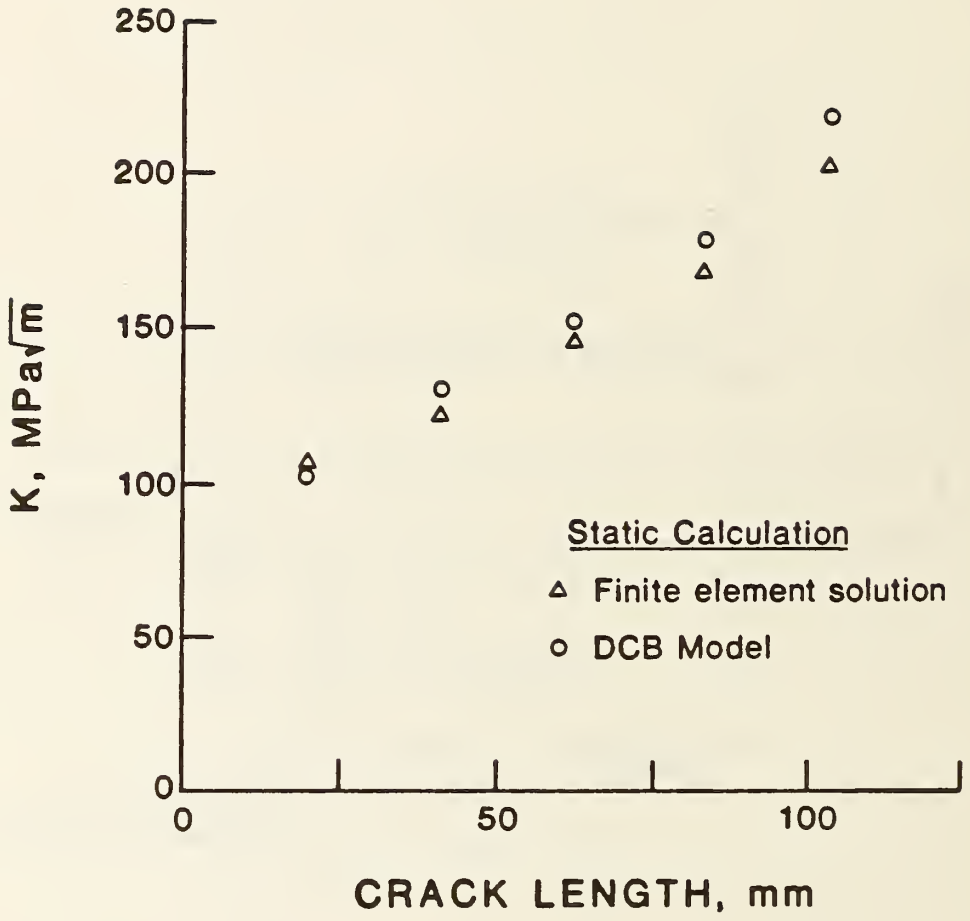

Figure 7. Comparison of static results for the stress intensity factor from one-dimensional beam model and two-dimensional finite element model.

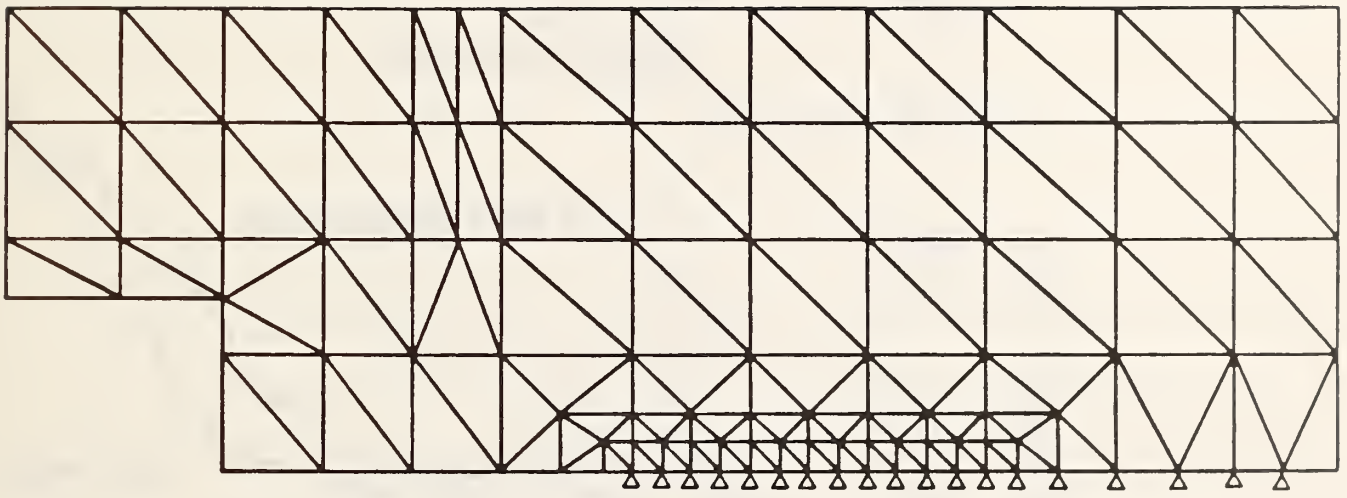

Figure 8. Finite element mesh used for dynamic analysis of DCB specimen.

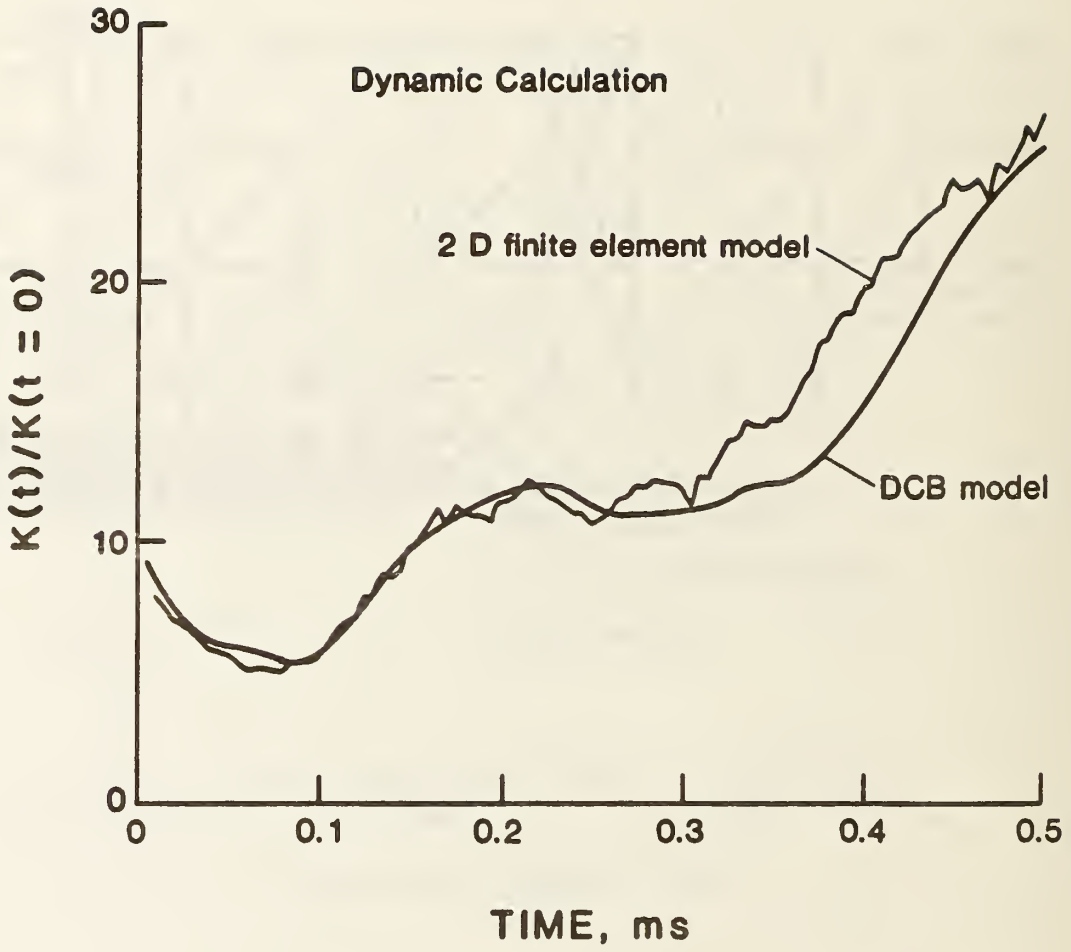

Figure 9. Comparison of results for K as a function of time from one-dimensional beam model and two-dimensional finite element model.

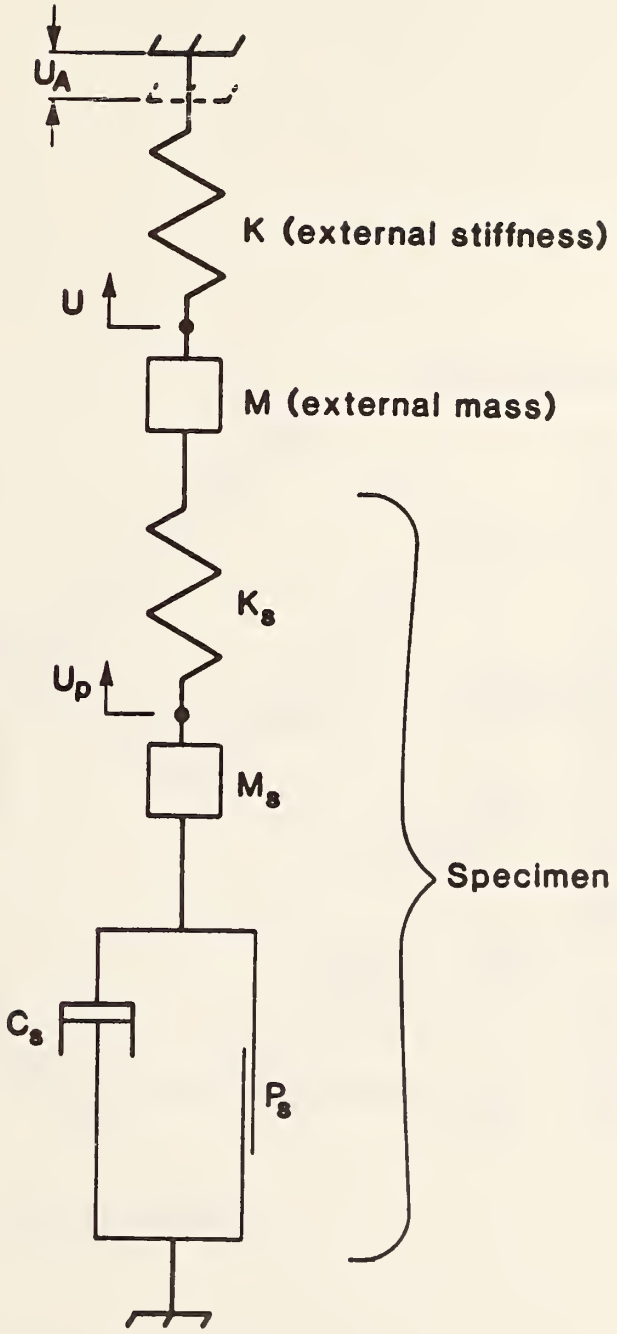

Figure 10. Lumped-mass visco-elastic-plastic dynamic model of DCB specimen.

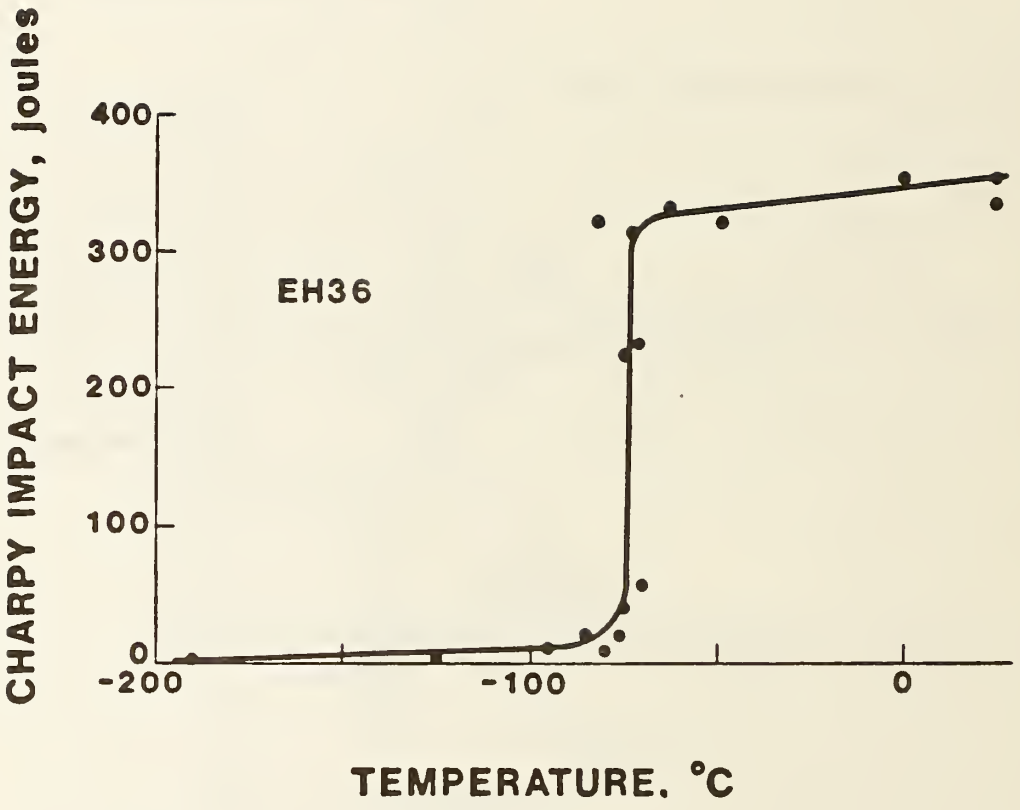

Figure 11. Ductile-to-brittle transition curve for EH36.

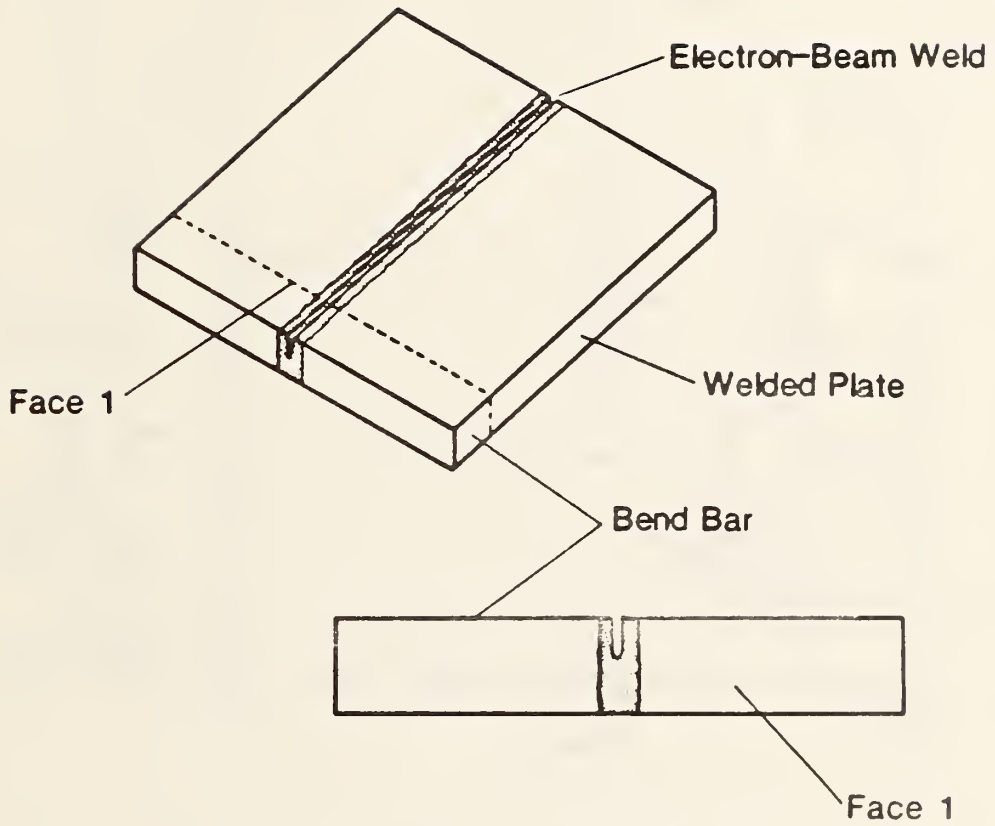

Figure 12. Three-point bend bars for static fracture toughness testing of electron beam welds.

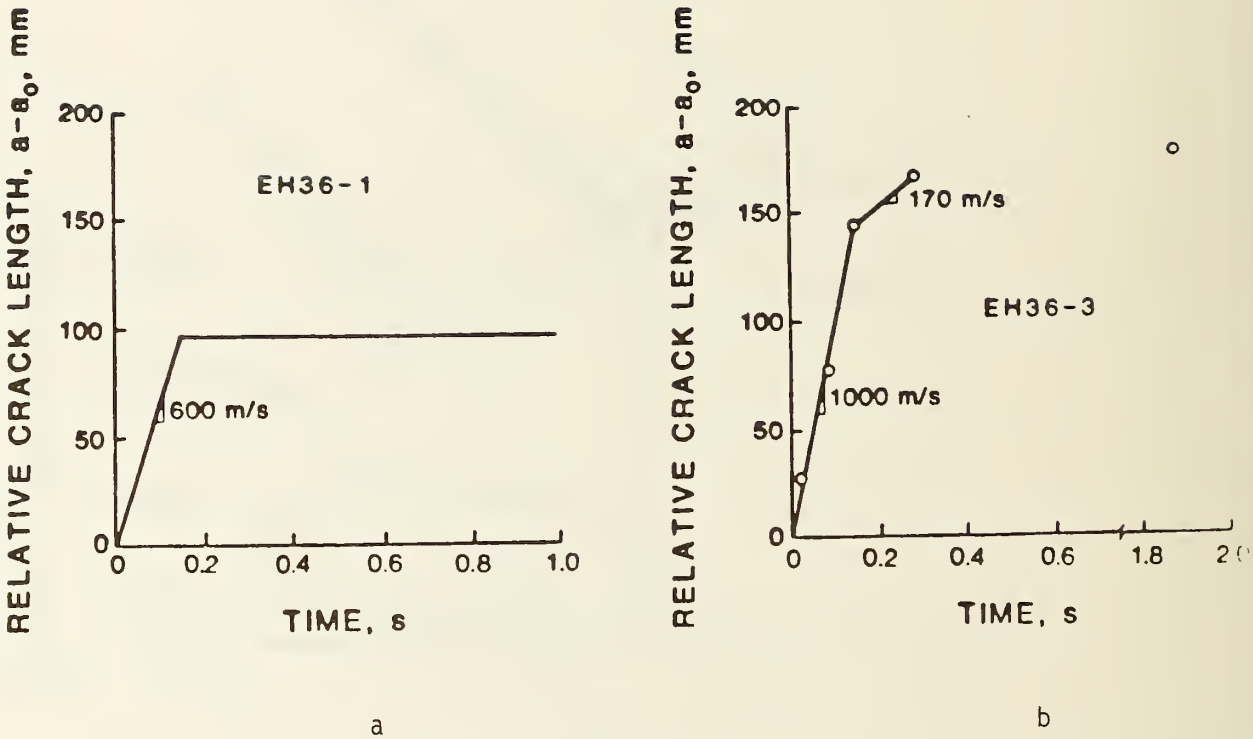

Figure 13. Crack speed as a function of time in EH36 tests.
(a) Test EH36-1 (b) Test EH36-3
(Individual crack detector gage breaks were not detectable in test EH36-1. Fig. 13(a) is inferred from calibration curve for crack gage circuit).

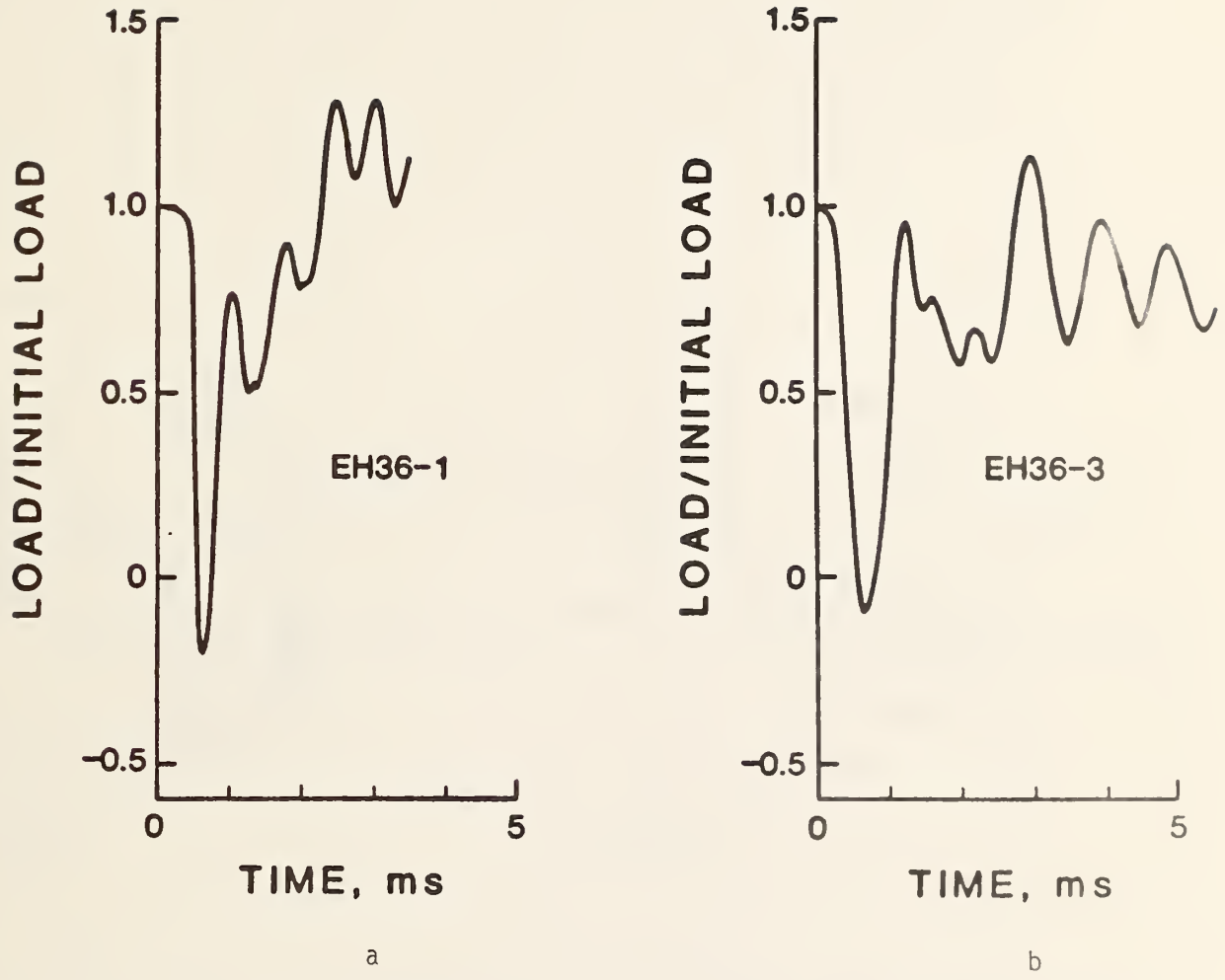

Figure 14. Applied load as a function of time in EH36 tests.
(a) Test EH36-1 (b) Test EH36-3.

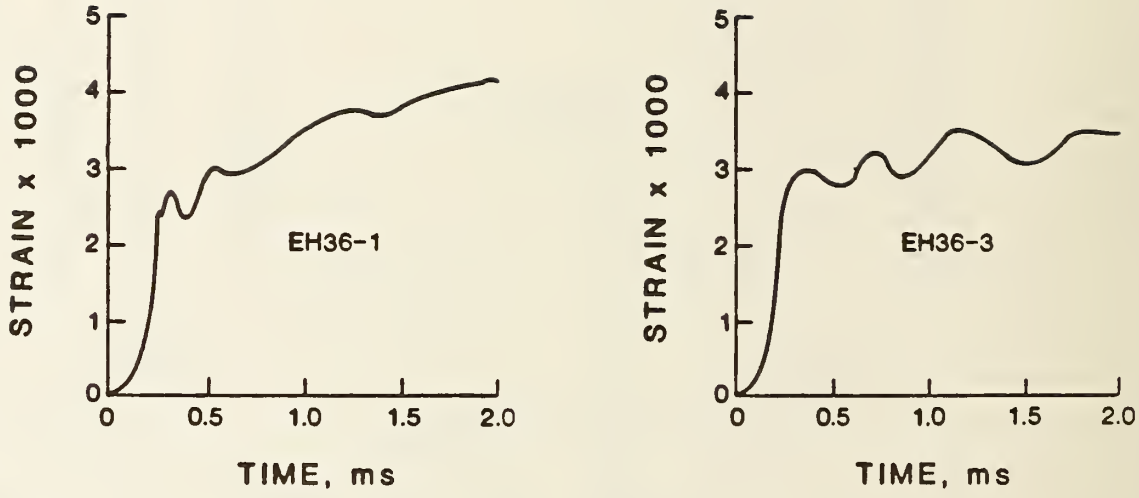

(a) Test EH36-1

(b) Test EH36-3

Figure 15. Strain in the vicinity of the end of the electron-beam weld in EH36 tests.

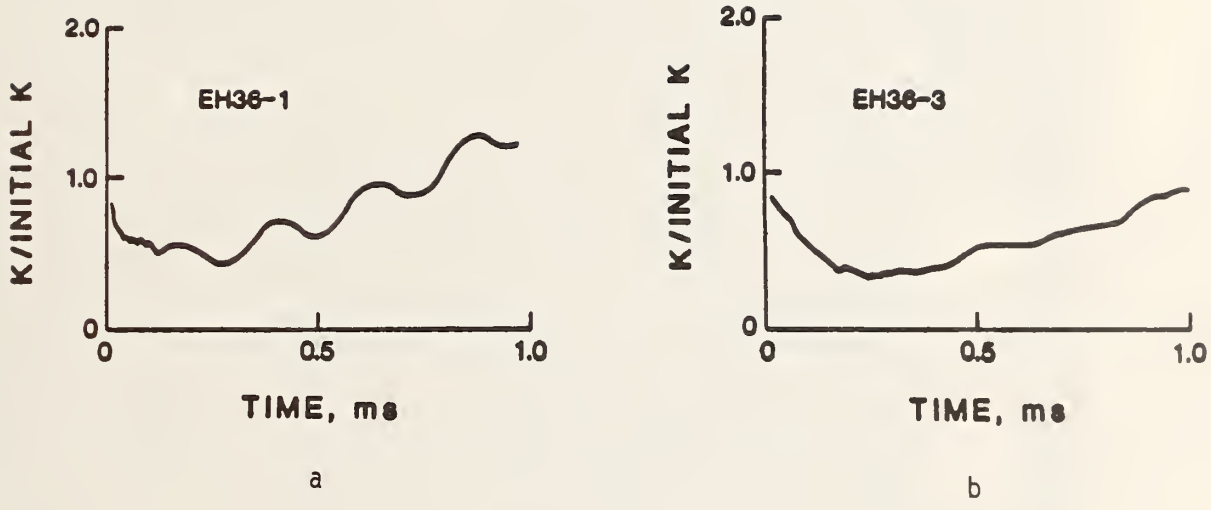

Figure 16. Dynamic stress intensity K as a function of time, calculated from the DCB model using observed crack velocity data, for specimens EH36-1 and EH36-3.

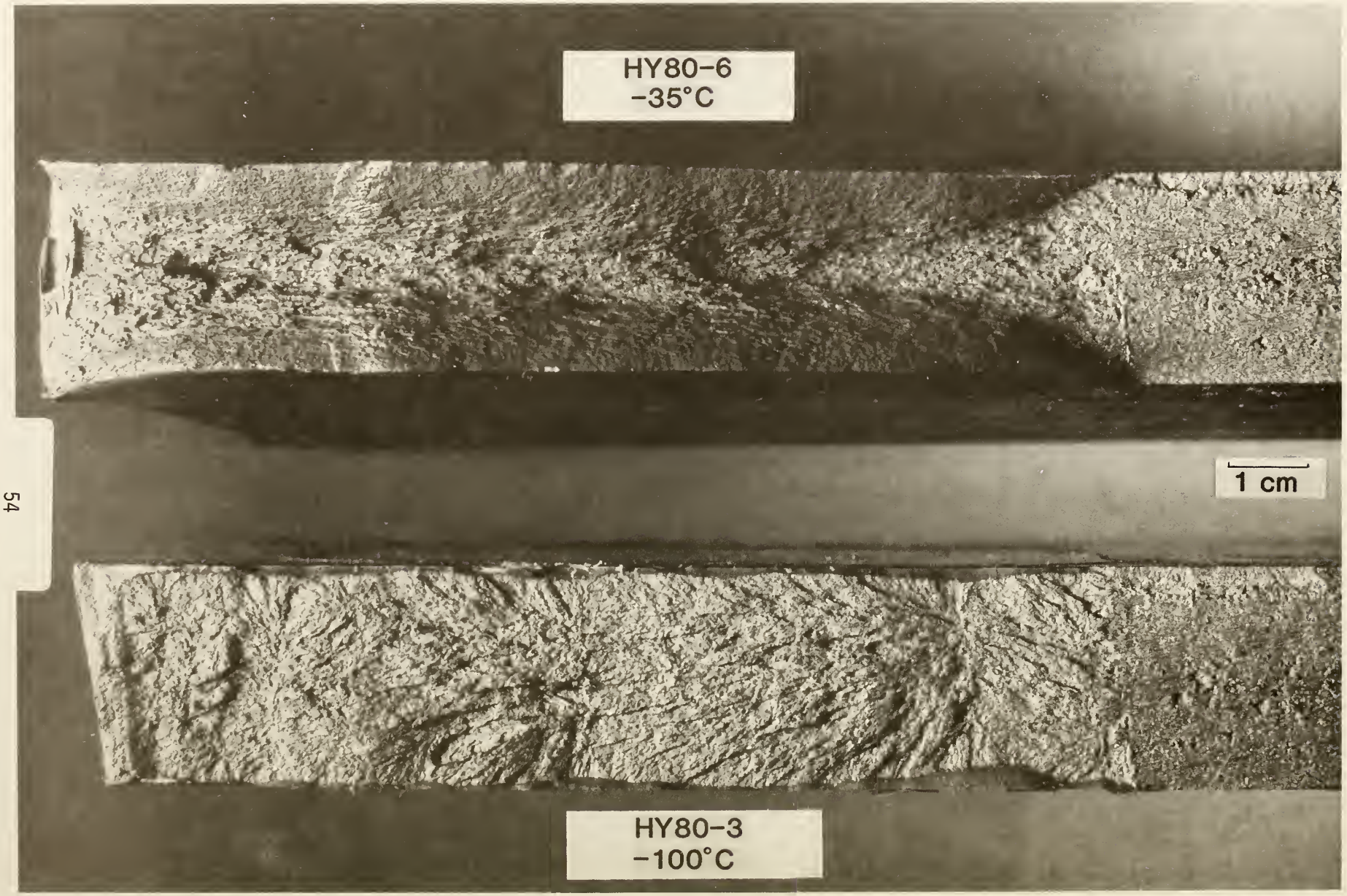

Figure 17. Typical fracture surfaces for HY80 DCB specimens.

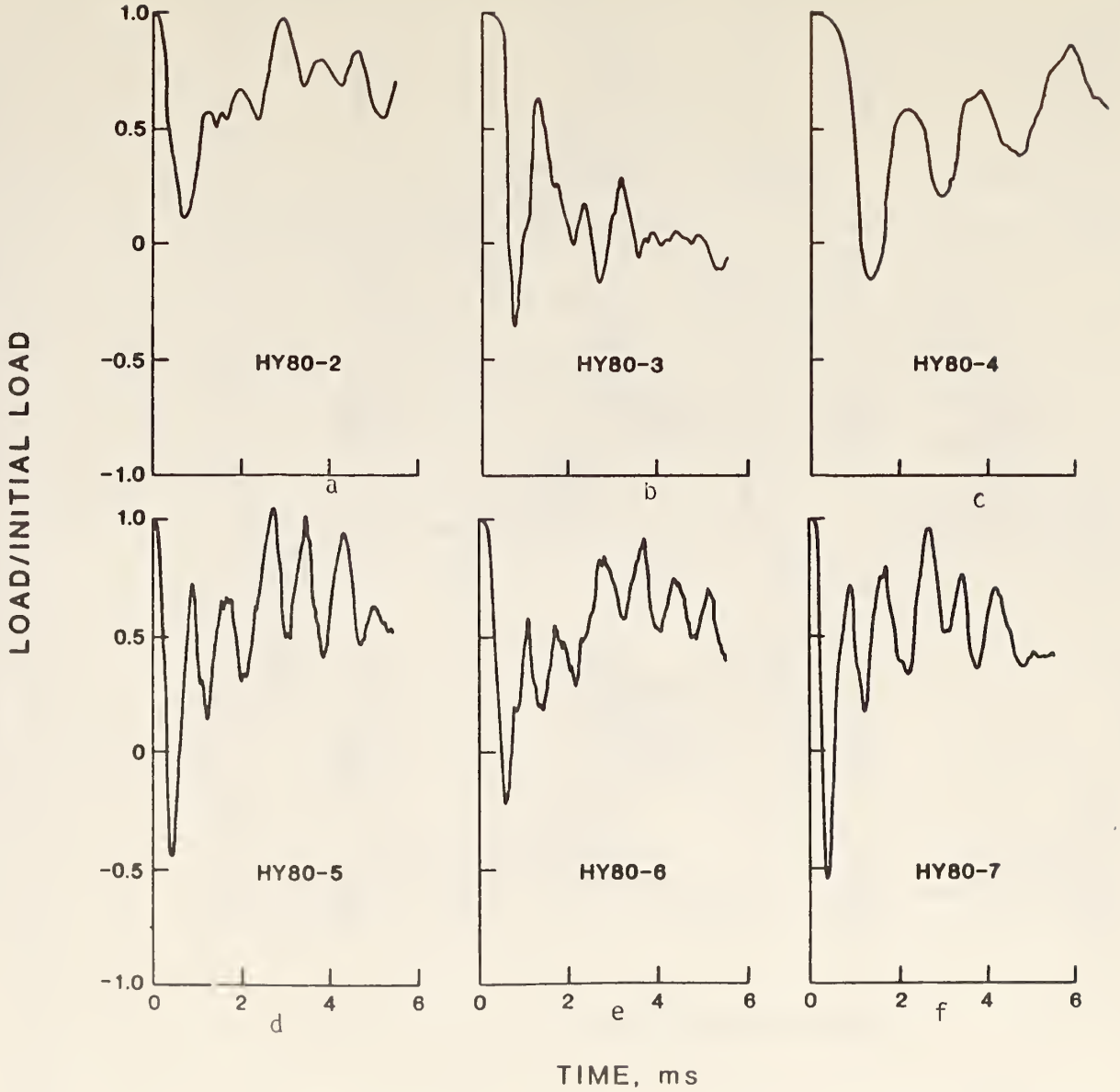

Figure 18. Crack position as a function of time inferred from crack detector gage traces for HY80 specimens.
(a) - (f) Tests HY80 2-7 respectively.
(Crack gage output was noisy in Tests 3 and 7. Figs. 18b and 18e are estimated).

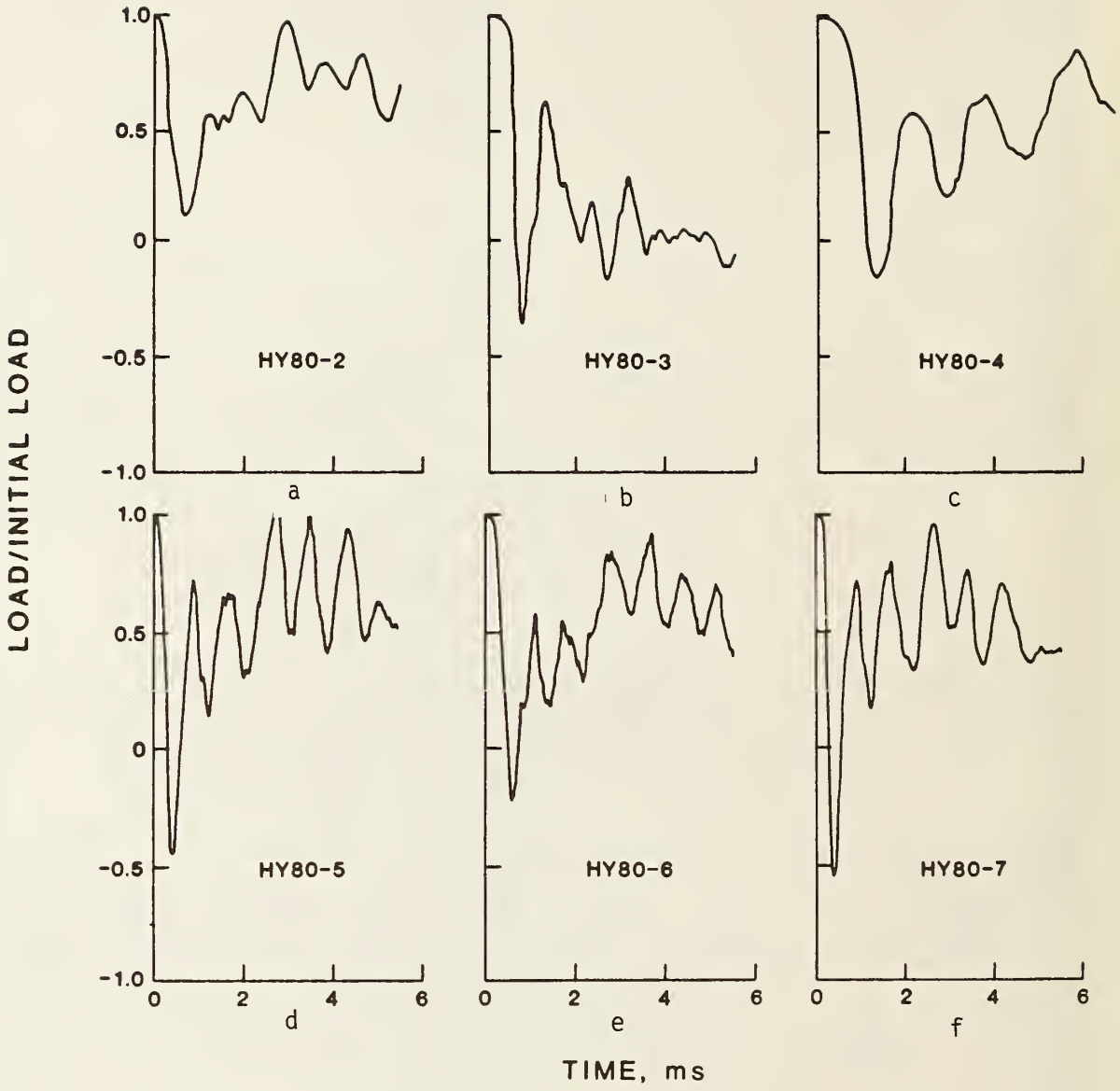

Figure 19. Applied load as a function of time in HY80 tests. (a) - (f) Tests HY80 2-7 respectively.

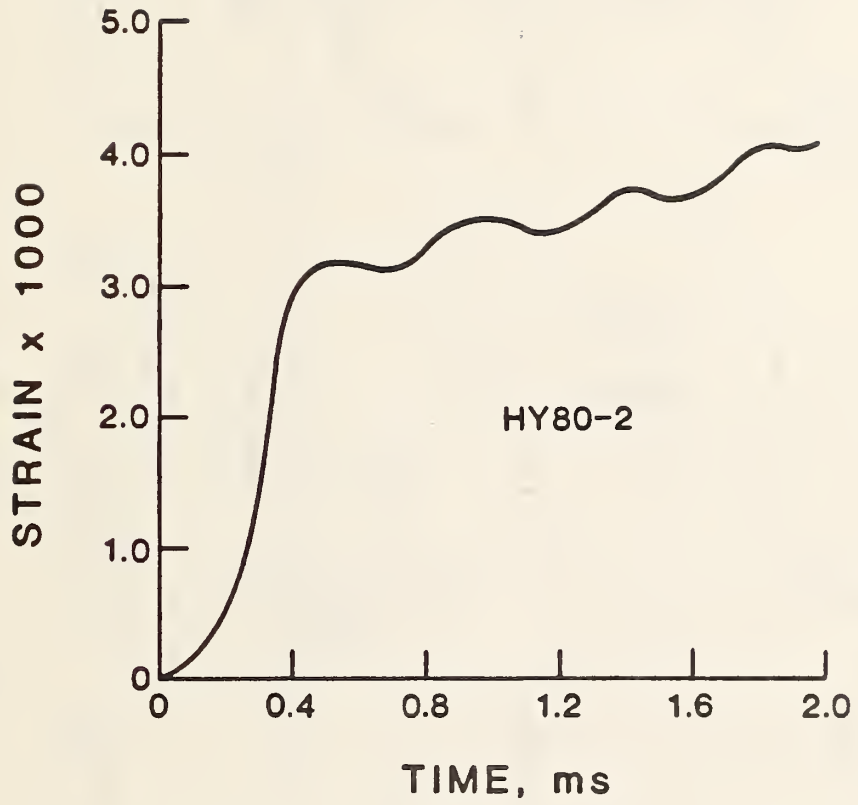

Figure 20. Strain in the vicinity of the end of the electron-beam weld along slip-band path in test HY80-2.

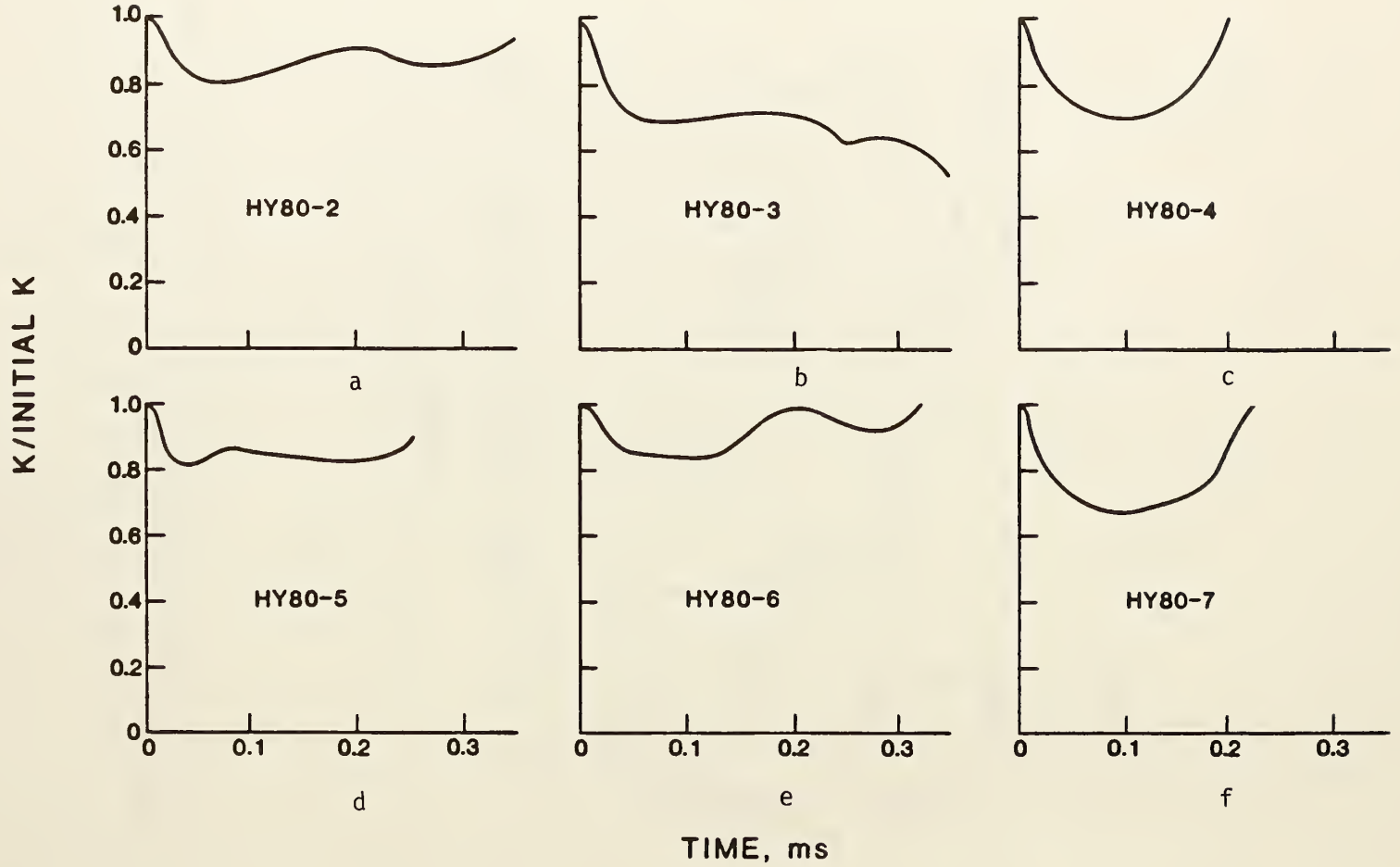

Figure 21. K as a function of time calculated from crack velocity data for HY80 tests. (a) - (f) Tests HY80 2-7 respectively.

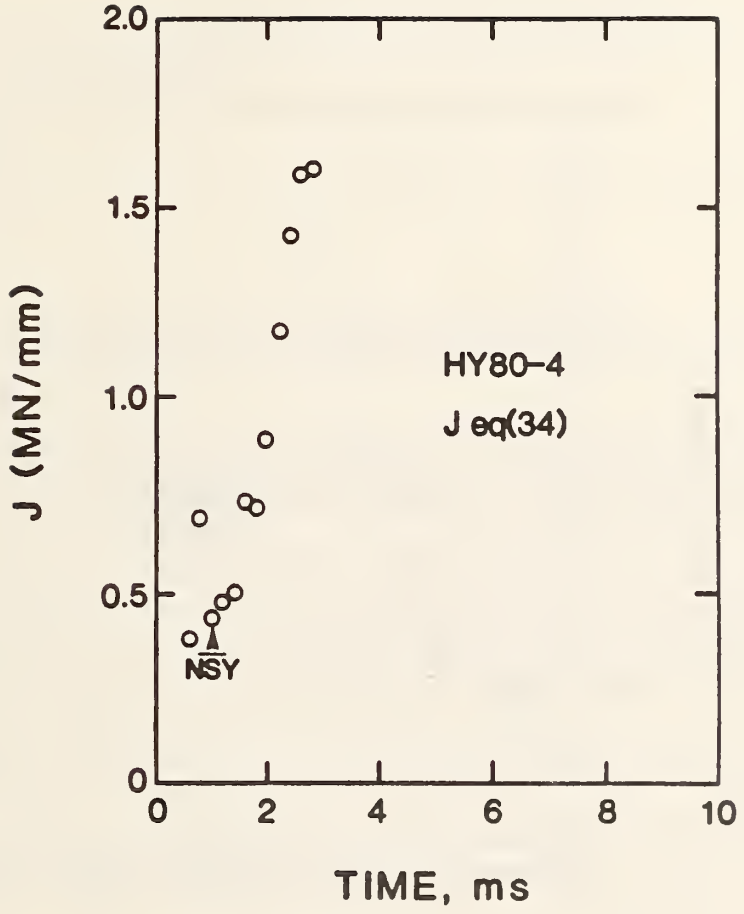

Figure 22. J-interval vs. time for HY80-4.

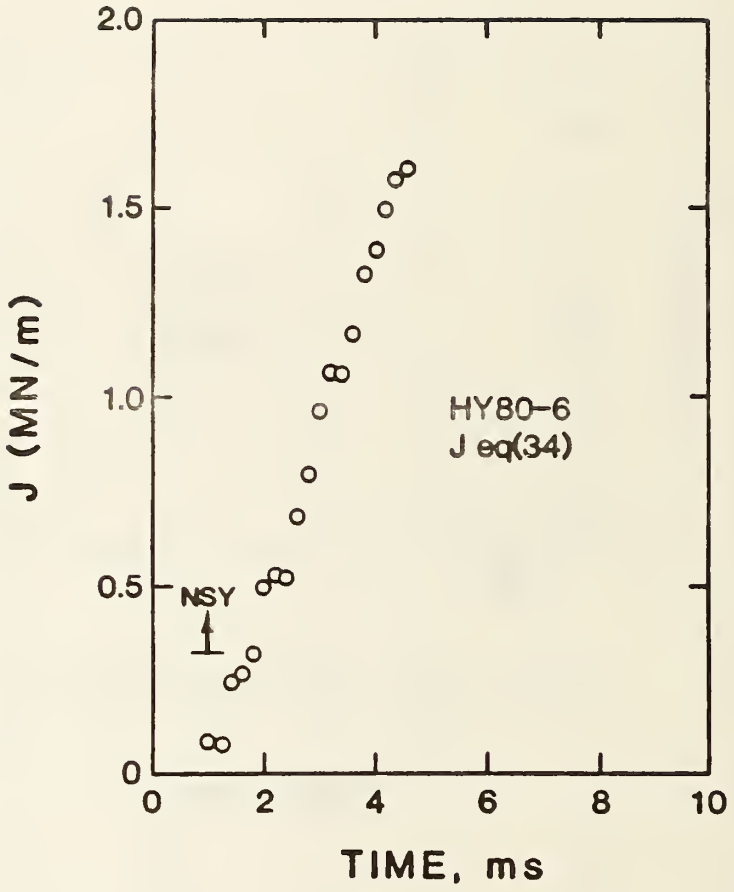

Figure 23. J-integral vs. time for HY80-6.

NBS-114A (REV. 2-8C)

U.S. DEPT. OF COMM. BIBLIOGRAPHIC DATA SHEET (See instructions)	1. PUBLICATION OR REPORT NO. NBSIR 84-3012	2. Performing Organ. Report No.	3. Publication Date October 1984

4. TITLE AND SUBTITLE

Materials Selection Criteria for Crack Arrester Strakes in Naval Vessels: Second Interim Progress Report

5. AUTHOR(S)

R. B. King, T. Teramoto, D. T. Read

6. PERFORMING ORGANIZATION (If joint or other than NBS, see instructions)

NATIONAL BUREAU OF STANDARDS
DEPARTMENT OF COMMERCE
WASHINGTON, D.C. 20234

7. Contract/Grant No.

8. Type of Report & Period Covered

9. SPONSORING ORGANIZATION NAME AND COMPLETE ADDRESS (Street, City, State, ZIP)

Naval Sea Systems Command SEA05R25
David Taylor Naval Ship Research and Development Center
Annapolis, MD 21402

10. SUPPLEMENTARY NOTES

☐ Document describes a computer program; SF-185, FIPS Software Summary, is attached.

11. ABSTRACT (A 200-word or less factual summary of most significant information. If document includes a significant bibliography or literature survey, mention it here)

The phenomenon of crack arrest, in which a crack propagates through a brittle material, encounters a high toughness material, and stops has been studied. This phenomenon is of practical importance in understanding crack arrest in ship structures. Laboratory experiments have been conducted under conditions intended to simulate those in a structural situation.

These experiments were designed to include two key features of ship structural behavior: 1) Crack arrest occurs specifically because a step in toughness is encountered; 2) the load on the specimen, simulating dead load in the structure, is transferred to the uncracked ligament after arrest, thus introducing the possibility of reinitiation. A spring-loaded double-cantilever-beam (DCB) specimen has been used in these experiments. An electron-beam weld is made along the crack propagation line, producing a brittle crack propagation path with a step in toughness at its end.

The dynamic run-arrest portion of these experiments has been modeled using a modification of Kanninen's DCB model that includes the effect of the loading spring, and using a finite element model. The elastic-plastic reloading portion has been modeled quasi-statically using J integral and tearing instability theory. In addition, a simplified dynamic viscoelastic-plastic model has been developed to analyze the reloading portion of the experiments.

Results of this program are intended to indicate quantitatively whether a candidate arrester material will arrest a crack at service temperatures and subsequently prevent reinitiation.

12. KEY WORDS (Six to twelve entries; alphabetical order; capitalize only proper names; and separate key words by semicolons)

crack arrest; crack propagation; dynamic fracture; dynamic toughness; elastic-plastic fracture; toughness

13. AVAILABILITY

☒ Unlimited

☐ For Official Distribution. Do Not Release to NTIS

☐ Order From Superintendent of Documents, U.S. Government Printing Office, Washington, D.C. 20402.

☒ Order From National Technical Information Service (NTIS), Springfield, VA. 22161

14. NO. OF PRINTED PAGES

64

15. Price

$10.00